iScience

CellPress
OPEN ACCESS

Article

# Highly efficient generation of self-renewing trophoblast from human pluripotent stem cells

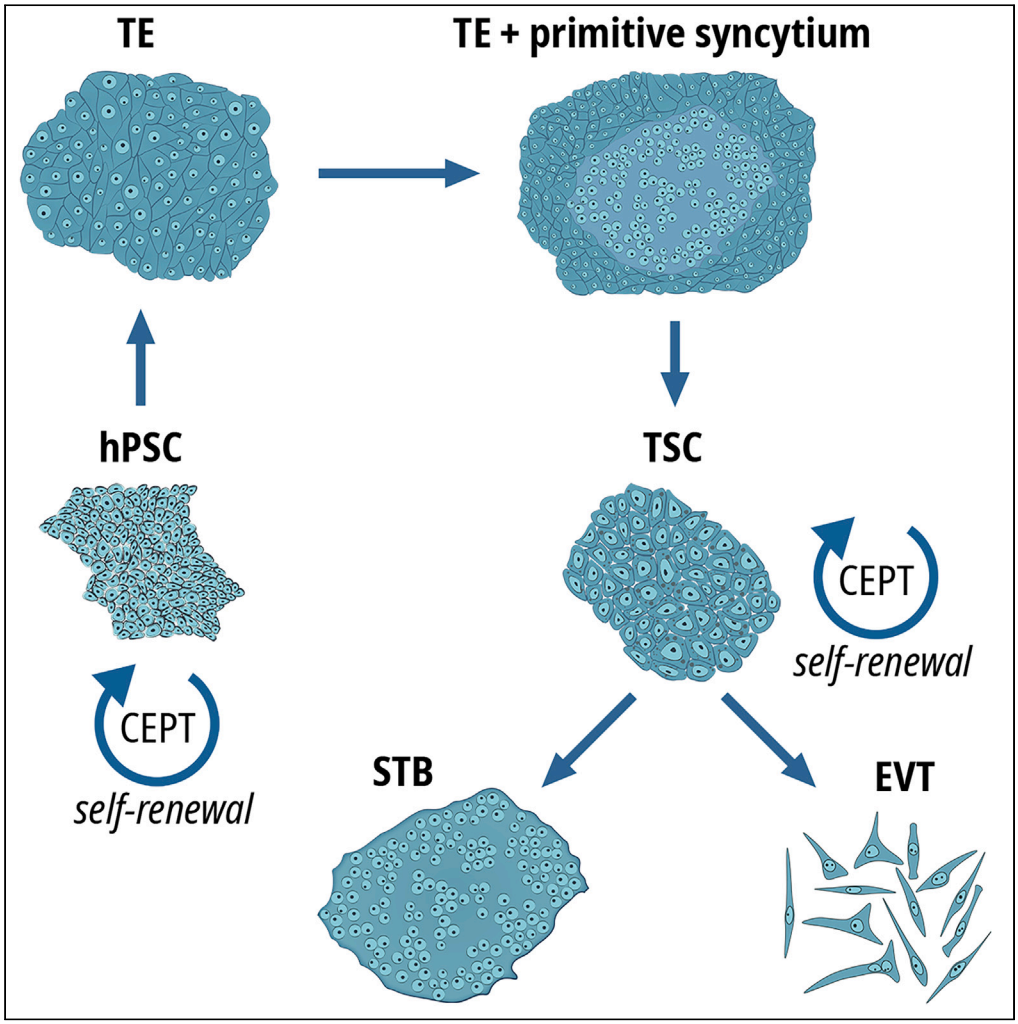


Jaroslav Slamecka, Seungmi Ryu, Carlos A. Tristan, ..., Ty C. Voss, Anton Simeonov, Ilyas Singeç

ilyassingec@gmail.com

## Highlights

Serum-free method for trophectoderm and trophoblast differentiation from hPSCs

Generation and functional characterization of four different trophoblast cell types

Long-term expansion and differentiation of trophoblast stem cells

Multi-omics analysis and comparison to first-trimester placenta

Slamecka et al., iScience 27, 110874
October 18, 2024 
https://doi.org/10.1016/j.isci.2024.110874

iScience

CellPress
OPEN ACCESS

Article

# Highly efficient generation of self-renewing trophoblast from human pluripotent stem cells

Jaroslav Slamecka,[1] Seungmi Ryu,[1] Carlos A. Tristan,[1] Pei-Hsuan Chu,[1] Claire Weber,[1] Tao Deng,[1] Yeliz Gedik,[1] Pinar Ormanoglu,[1] Ty C. Voss,[1] Anton Simeonov,[1] and Ilyas Singeç[1,2,3,*]

## SUMMARY

**Human pluripotent stem cells (hPSCs) represent a powerful model system to study early developmental processes. However, lineage specification into trophectoderm (TE) and trophoblast (TB) differentiation remains poorly understood, and access to well-characterized placental cells for biomedical research is limited, largely depending on fetal tissues or cancer cell lines. Here, we developed novel strategies enabling highly efficient TE specification that generates cytotrophoblast (CTB) and multinucleated syncytiotrophoblast (STB), followed by the establishment of trophoblast stem cells (TSCs) capable of differentiating into extravillous trophoblast (EVT) and STB after long-term expansion. We confirmed stepwise and controlled induction of lineage- and cell-type-specific genes consistent with developmental biology principles and benchmarked typical features of placental cells using morphological, biochemical, genomics, epigenomics, and single-cell analyses. Charting a well-defined roadmap from hPSCs to distinct placental phenotypes provides invaluable opportunities for studying early human development, infertility, and pregnancy-associated diseases.**

## INTRODUCTION

The inaccessibility of human tissue at early embryonic stages remains a major challenge for the study of placental development and function in health and disease. Typically, TSCs are isolated either from blastocyst-stage embryos or first-trimester placental villi.[1,2] Derivation of TSCs from these sources is not only limiting for systematic studies but also ethically problematic. Human induced pluripotent stem cells (iPSCs) represent an attractive and scalable source for cell types of the embryonic germ layers (ectoderm, mesoderm, endoderm). Recent work suggested that iPSCs may also produce extra-embryonic cell types such as trophoblast and amnion.[3–6] However, key questions and controversies remain about the basic biology and potential translational utility of iPSC-derived phenotypes representing extra-embryonic tissues.

A hallmark of early mammalian development is lineage segregation into TE and the inner cell mass (ICM). TE will generate the placenta as the critical organ of pregnancy, whereas the post-implantation ICM gives rise to the epiblast (embryo proper) and primitive endoderm.[7] Cultured hPSCs show molecular features of primed pluripotency, resembling the post-implantation epiblast that can generate the primary embryonic germ layers.[7] However, some studies suggested that primed or conventional hPSCs might differentiate into TE or express TE-associated genes upon treatment with BMP4 either alone[8–10] or in combination with inhibitors of TGF-β and FGF signaling.[3,4,11–13] Other reports challenged these observations suggesting partial TE differentiation or generation of extra-embryonic mesoderm.[14–16] More recent efforts to generate extra-embryonic lineages from hPSCs focused on cells with enhanced potency, so-called naive pluripotency[17–20], or isolation of TE-competent cells during cellular reprogramming into iPSCs.[21,22] Here, we report highly efficient and rapid differentiation of hPSCs, routinely cultured in chemically defined E8 medium, into early TB cells and self-renewing TSCs that can be further differentiated into STB and EVT. Importantly, our protocols are reproducible with several hPSC lines, avoid genetic manipulation, and do not require the detour from primed-to-naive pluripotency. We provide deep cell characterization using genomic and epigenomic methods, perform multiple comparisons (e.g., first-trimester placenta, embryonic germ layers), and establish a rich resource for data mining and scalable manufacturing of human placental cells for reproducible translational research.

## RESULTS

### Lineage specification into trophectoderm

TE develops as an extra-embryonic epithelial layer consisting of mononuclear CTB and multinucleated STB that anchor the implanting embryo to the decidua. To initiate TE differentiation, hPSCs cultured in E8 medium were switched to TE1 medium, which is E6 medium

[1]National Center for Advancing Translational Sciences (NCATS), Division of Preclinical Innovation, Stem Cell Translation Laboratory (SCTL), National Institutes of Health (NIH), Rockville, MD 20850, USA
[2]Present address: FUJIFILM Cellular Dynamics Inc., Madison, WI, USA
[3]Lead contact
*Correspondence: ilyassingec@gmail.com
https://doi.org/10.1016/j.isci.2024.110874

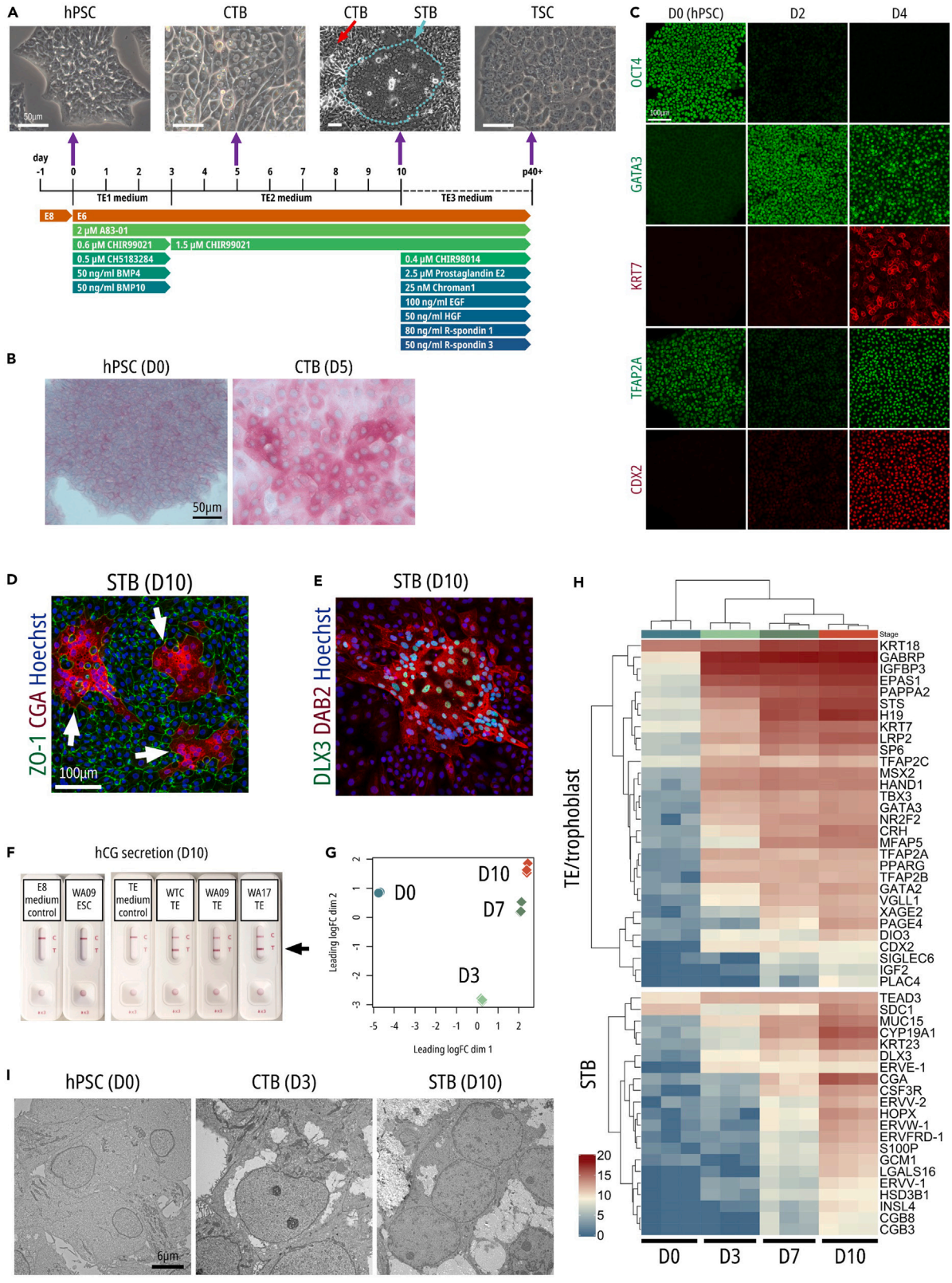
A
hPSC
CTB
CTB
STB
TSC
50μm
day
-1
0
1
2
3
4
5
6
7
8
9
10
p40+
TE1 medium
TE2 medium
TE3 medium
E8
E6
2 μM A83-01
0.6 μM CHIR99021
1.5 μM CHIR99021
0.5 μM CH5183284
50 ng/ml BMP4
50 ng/ml BMP10
0.4 μM CHIR98014
2.5 μM Prostaglandin E2
25 nM Chroman1
100 ng/ml EGF
50 ng/ml HGF
80 ng/ml R-spondin 1
50 ng/ml R-spondin 3
B
hPSC (D0)
CTB (D5)
50μm
C
D0 (hPSC)
D2
D4
OCT4
GATA3
KRT7
TFAP2A
CDX2
100μm
D
STB (D10)
ZO-1 CGA Hoechst
100μm
E
STB (D10)
DLX3 DAB2 Hoechst
F
hCG secretion (D10)
E8 medium control
WA09 ESC
TE medium control
WTC TE
WA09 TE
WA17 TE
G
D10
D0
D7
D3
Leading logFC dim 2
Leading logFC dim 1
H
Stage
TE/trophoblast
STB
KRT18
GABRP
IGFBP3
EPAS1
PAPPA2
STS
H19
KRT7
LRP2
SP6
TFAP2C
MSX2
HAND1
TBX3
GATA3
NR2F2
CRH
MFAP5
TFAP2A
PPARG
TFAP2B
GATA2
VGLL1
XAGE2
PAGE4
DIO3
CDX2
SIGLEC6
IGF2
PLAC4
TEAD3
SDC1
MUC15
CYP19A1
KRT23
DLX3
ERVE-1
CGA
CSF3R
ERVV-2
HOPX
ERVW-1
ERVFRD-1
S100P
GCM1
LGALS16
ERVV-1
HSD3B1
INSL4
CGB8
CGB3
20
15
10
5
0
D0
D3
D7
D10
I
hPSC (D0)
CTB (D3)
STB (D10)
6μm

**Figure 1. Morphology and characterization of early TE cells**

(A) Overview of the strategy to differentiate hPSCs into TE, TB, and self-renewing TSCs. Phase-contrast images correspond to select time points. Scale bars: 50 μm.
(B) Periodic Acid-Schiff (PAS) staining showing strongly increased glycogen deposits in TE/CTB versus undifferentiated hPSC (WA09). Scale bar: 50 μm.
(C) Immunocytochemistry shows directed differentiation of iPSCs into TE (JHU198i line). Scale bar: 100 μm.
(D and E) TE cultures at day 10 (D10) with marker expression characteristic of STB cells. Scale bar: 100 μm.
(F) hCG secretion into the culture medium was confirmed by a pregnancy test in D10 TE cells derived from 3 different cell lines.
(G) MDS plot showing gradual changes in the transcriptional profiles of WA09 ESCs differentiating into TB.
(H) Heatmap of the selected most highly differentially expressed genes between D0 and D10 (log fold change >8.5, FDR-adjusted $p$ value $<1 \times 10^{-4}$).
(I) Representative TEM images of TE cultures at D3 and D9 of differentiation along with ESC (WA09) control (D0). Scale bar: 6 μm.

supplemented with a combination of A83-01 (TGF-β inhibitor), CHIR99021 (GSK-3 inhibitor), CH5183284 (FGFR inhibitor), BMP4, and BMP10 (Figure 1A). BMP4 was previously used to induce trophoblastic properties in hPSCs,[8–10,12] while other BMP isoforms such as BMP10 were also tested and used for trophoblast derivation.[23] TE1 culture conditions resulted in rapid morphological changes and the emergence of cells with a cytoplasm appearing dark in phase-contrast microscopy (Figure 1A). Periodic Acid-Schiff (PAS) staining showed the cytoplasmic accumulation of large glycogen deposits, characteristic of early trophoblast[24] (Figure 1B). Withdrawal of BMPs, CH5183284, and an increased concentration of CHIR99021 on day 3 (denoted as TE2 medium) then led to further epithelial differentiation and spontaneous formation of primitive syncytium-like structures by a small subset of cells (Figure 1A). Subsequently, we established long-term, self-renewing TSC lines from the TE/CTB cells by switching to TE3 medium (described later in Figures 3, 4, 5, 6, and 7).

As early as day 2 after TE1 medium application, the pluripotency-associated transcription factor OCT4 (POU5F1) was rapidly downregulated and GATA3, a pioneering TE specifier,[9,25,26] was strongly induced as shown by immunocytochemistry (Figure 1C). Additional TE markers including KRT7, TFAP2A, and CDX2[9,25] were induced by day 4 (Figure 1C). Of note, immunocytochemical analysis of TFAP2A in hPSCs showed a differential staining pattern including the prominent labeling of nucleoli in some cells, then briefly disappeared on day 2 of differentiation and was again detectable on day 4 showing the homogeneous staining of virtually all nuclei (Figure 1C).

Between days 7–10, the monolayer of ZO-1 expressing TE/CTB cells (Figure 1D) spontaneously fused into large multinucleated STB-like structures (Figures 1A, 1D, 1E, and S1A–S1D; Video S1), resembling primitive syncytium of the peri-implantation stage human embryo.[27] Human chorionic gonadotropin (hCG) is a critical pregnancy hormone and its α subunit, CGA, was specifically induced by STB (Figure 1D). Similarly, STB markers DAB2 and DLX3[28] (www.proteinatlas.org) were detected by immunocytochemistry (Figures 1E and S1B). Image-based quantification showed that approximately 5.5% of total cells were DLX3-positive after using the complete TE1 medium, whereas omitting BMP10 and CH5183284 or BMP4 from the TE1 medium during TE induction (days 0–3) had a negative effect on the generation of DLX3-expressing STB (Figure S1C). KRT18 is expressed in morula- and blastocyst-stage TE[29] and was strongly expressed by both TE/CTB and STB cells (Figure S1D). Next, the use of an over-the-counter pregnancy test confirmed the secretion of hCG into the supernatants of TE/CTB cells derived from three hPSC lines at day 10 and its absence in human embryonic stem cell (hESC) cultures and medium controls devoid of any cells (Figure 1F). LC-MS/MS-based secretome analysis of supernatants confirmed the enrichment of CGB1 (chorionic gonadotropin subunit β1) and CGA peptide subunits by TB but not hPSC cultures (Table S1).

Next, we performed time-course RNA sequencing (RNA-seq) analysis of hPSCs (D0) and differentiating TB cells harvested on days 3, 7, and 10. Multidimensional scaling (MDS) showed distinct clustering of samples across different timepoints (Figure 1G). Early TE genes and STB markers were gradually upregulated (Figure 1H; Table S2), whereas pluripotency-associated genes were downregulated (Table S2). Of note, the induction of the fusogenic human endogenous retroviral genes *ERVW1* (syncytin-1) and *ERVFRD-1* (syncytin-2), known to participate in trophoblast fusion,[30] correlated with the emergence of STB at day 7–10 (Figure 1H).

Ultrastructural analysis using transmission electron microscopy (TEM) showed cell type-specific characteristics of pluripotent and differentiating cells. hPSCs displayed typical features of unspecialized cells, such as round, homogeneous nuclei and few organelles surrounded by granular cytoplasm (Figures 1I and S1E). By day 3, TE/CTB cells formed desmosomes, nuclei displayed prominent nucleoli, and their cytoplasm contained large amounts of rough ER (rER) and mitochondria. On day 10, large multinucleated STB structures were observed showing well-developed rER, mitochondria, microfilaments, Golgi apparatus, and large cytoplasmic vacuoles consistent with the identity and function of secretory placental cells.

Based on the findings described above, we decided to revisit previous approaches, which used BMP4 alone or in combination with A83-01 and PD173074 (known as the BAP protocol) to induce trophoblast properties in hPSC.[8–10,12] When comparing these conditions to our method, all three treatments generated cells with distinct morphologies (Figures S1F and S1G). Interestingly, TE1/TE2 media strongly induced the expression of CDX2, which was absent in BAP-treated cultures and sporadically expressed in a few cells after the application of BMP4 only. Of note, BMP4 alone led to the induction of the mesodermal marker brachyury (TBXT) and showed residual expression of OCT4 (Figure S1F). Altogether, TE1/TE2 treatment was optimal for TE induction and our findings may in part explain the controversy in the literature when using BMP4 only or the BAP protocol.

Lastly, we used flow cytometry as an independent method to compare undifferentiated hPSCs (D0) to TE (D10). Upon differentiation, virtually all cells expressed the TE markers EGFR, ENPEP, and TACSTD2 (TROP2) (Figure S2). Taken together, we established a robust and stepwise differentiation method for hPSCs cultured in E8 medium that recapitulates the early stages of TE differentiation.

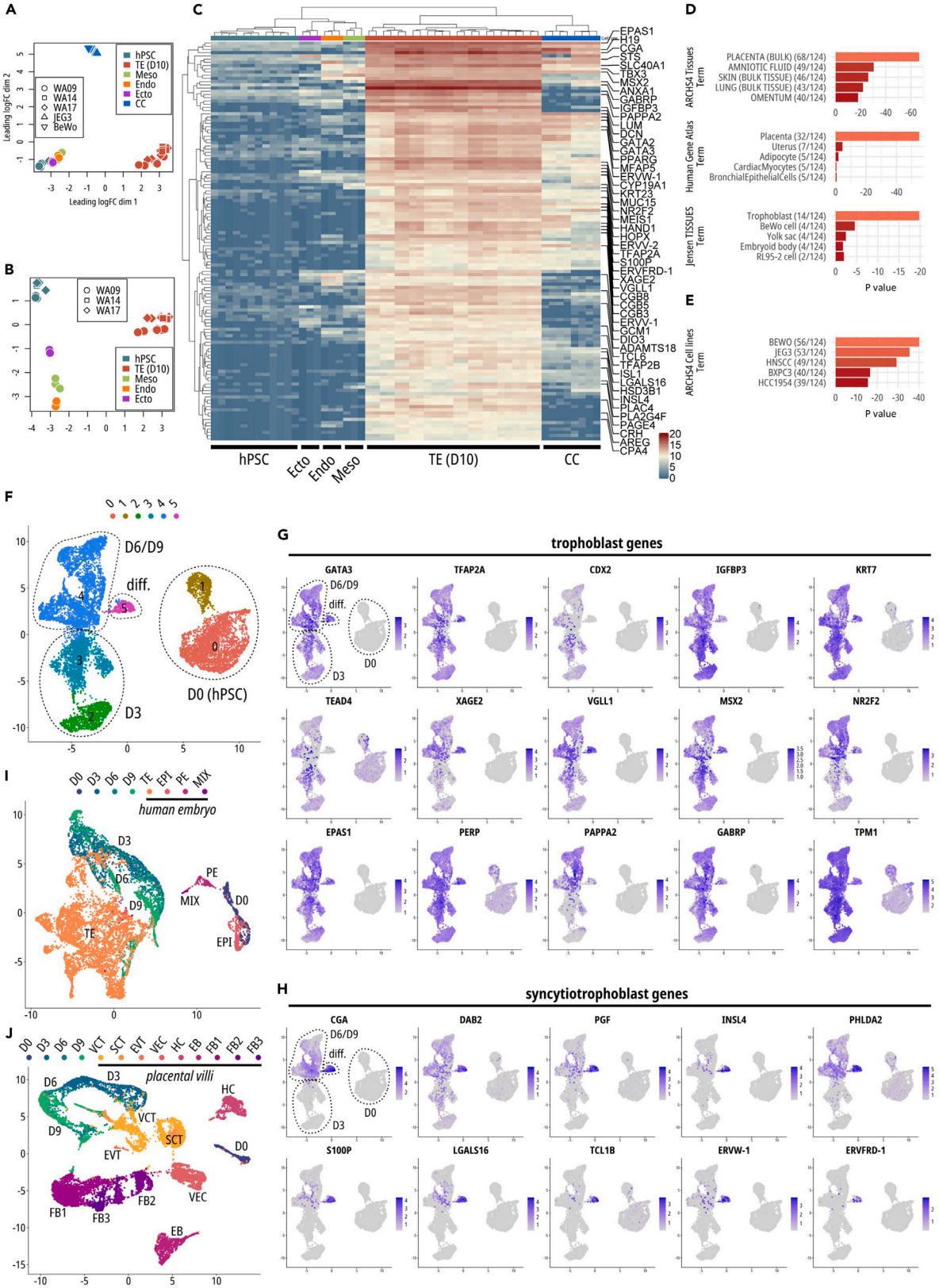
A
B
C
D
E
F
G
H
I
J
hPSC
TE (D10)
Meso
Endo
Ecto
CC
WA09
WA14
WA17
JEG3
BeWo
Leading logFC dim 1
Leading logFC dim 2
EPAS1
H19
CGA
STS
SLC40A1
TBX3
MSX2
ANXA1
GABRP
IGFBP3
PAPPA2
LUM
DCN
GATA2
GATA3
PPARG
MFAP5
ERVW-1
CYP19A1
KRT23
MUC15
NR2F2
MEIS1
HAND1
HOPX
ERVV-2
TFAP2A
S100P
ERVFRD-1
XAGE2
VGLL1
CGB8
CGB5
CGB3
ERVV-1
GCM1
DIO3
ADAMTS18
TCL6
TFAP2B
ISL1
LGALS16
HSD3B1
INSL4
PLAC4
PLA2G4F
PAGE4
CRH
AREG
CPA4
ARCHS4 Tissues Term
PLACENTA (BULK) (68/124)
AMNIOTIC FLUID (49/124)
SKIN (BULK TISSUE) (46/124)
LUNG (BULK TISSUE) (43/124)
OMENTUM (40/124)
Human Gene Atlas Term
Placenta (32/124)
Uterus (7/124)
Adipocyte (5/124)
CardiacMyocytes (5/124)
BronchialEpithelialCells (5/124)
Jensen TISSUES Term
Trophoblast (14/124)
BeWo cell (4/124)
Yolk sac (4/124)
Embryoid body (4/124)
RL95-2 cell (2/124)
P value
ARCHS4 Cell lines Term
BEWO (56/124)
JEG3 (53/124)
HNSCC (49/124)
BXPC3 (40/124)
HCC1954 (39/124)
D6/D9
diff.
D3
D0 (hPSC)
trophoblast genes
GATA3
TFAP2A
CDX2
IGFBP3
KRT7
TEAD4
XAGE2
VGLL1
MSX2
NR2F2
EPAS1
PERP
PAPPA2
GABRP
TPM1
syncytiotrophoblast genes
CGA
DAB2
PGF
INSL4
PHLDA2
S100P
LGALS16
TCL1B
ERVW-1
ERVFRD-1
human embryo
placental villi
PE
MIX
EPI
VCT
SCT
EVT
VEC
HC
EB
FB1
FB2
FB3

**Figure 2. Analysis of the transcriptome of hPSC-derived TB cells included TB derived from three ESC lines (WA09, WA14, and WA17). D0 controls and WA09-derived endoderm (Endo), mesoderm (Meso), and ectoderm (Ecto) samples were included, as well as CC lines JEG-3 and BeWo.**

(A and B) MDS plots of the above ESC lines (A) with and (B) without CC lines included.

(C) Heatmap of the 124 most highly differentially expressed genes (log-fold change >8.5, FDR-adjusted $p$ value $<1 \times 10^{-4}$) between TB samples and hPSC samples.

(D) Enrichr analysis of the 124 differentially expressed genes displayed on the heatmap.

(E) Enrichr analysis – ARCHS4 database.

(F) UMAP plot of time-course scRNA-seq of WA09 hPSC differentiation into TB.

(G) UMAP plots are colored by the expression of individual differentially expressed TE or placenta-associated genes.

(H) Expression of markers associated with STB identity.

(I) Integration of the scRNA-seq data with data derived from human peri-implantation stage embryo[31] using the integration method in R package "Seurat."

(J) The same integration method with primary placental villi tissue.[32] VCT – villous cytotrophoblast, SCT – syncytiotrophoblast, EVT – extravillous trophoblast, FB – trophoblastic fibroblasts, VEC – vascular endothelial cells, EB – erythroblasts, HC – Hofbauer cells.

## Transcriptional landscape of human pluripotent stem cell-derived trophectoderm cells

We performed detailed systematic RNA-seq experiments to analyze TE cells in comparison to the three primary germ layers derived from the same parental hESC lines (WA09, WA14, WA17) as well as two choriocarcinoma (CC) cell lines, JEG-3 and BeWo. Differentiation into primary germ layers was performed using commercially available kits (STEMCELL Technologies) and cells expressed PAX6 (ectoderm), SOX17 (endoderm), or TBXT (mesoderm) (Figures S3A–S3C). MDS plots revealed that TE clustered away from hPSC and somatic lineages (Figure 2A). Cancer cell lines JEG3 and BeWo clustered distinctly from all hPSC-derived cell types, likely reflecting their abnormal identities. Excluding CC lines from the MDS plot allowed the visualization of the relationships between hPSC-derived cell types only, revealing a distinct path of the TE lineage (Figure 2B). Among the most highly differentially expressed genes between hPSC and TE were typical trophoblast markers (Table S3). STB markers were detected from the subpopulation of multinucleated STB (Figure 2C). Gene set enrichment analysis of the TE-associated genes showed "placenta" and "trophoblast" as top terms based on three databases (Figure 2D), while the most similar ARCHS4 cell lines identified were the CC lines BeWo and JEG-3 (Figure 2E). Downregulated genes in TE samples were markers of pluripotency, such as *OCT4*, *NANOG*, and *SOX2* (Figure S3A). As expected, the three germ layers (ectoderm, mesoderm, endoderm) derived from hPSCs expressed typical markers. Genes such as *HAVCR1*, *DNMT3L*, and *GTSF1* were specifically expressed in the CC lines (Figure S3A).

According to the Human Protein Atlas (HPA),[33–35] 91 genes and proteins are characteristic of the placenta. RNA-seq showed a high enrichment of these genes in hPSC-derived TE samples and to a lesser extent in CC lines while the number of these genes being expressed in hPSC and the three germ layers was low (Figure S3B). Similarly, genes that were recently associated with TE of human peri-implantation stage embryos[31] were enriched in hPSC-derived TE lines and CC lines but had limited expression in hPSC and the three germ layers (Figure S3C). In summary, this data revealed a distinct transcriptome of hPSC-derived TE cells.

## Single-cell analysis of trophectoderm differentiation

To characterize the differentiation process of pluripotent cells into TE, we performed time-course single-cell RNA-seq (scRNA-seq). The UMAP plot showed a clear separation between day 0 and day 3 samples, whereas day 6 and day 9 samples had more similar profiles (Figures 2F, S4A, and S4B). Marker genes identified in each cluster (Table S4) included known pluripotency genes at day 0 (Figure S4A) and indicated the acquisition of a TE signature in the remaining samples (Figure 2G). Among the differentially expressed genes between hPSC (D0) and TE samples were early TB markers and HPA core 91 placenta-specific markers. Pan-trophoblast markers *KRT7* and *PERP*[32] were strongly expressed. Differentiating cells in clusters 2, 3, and 4 could be distinguished based on the top 30 marker genes as shown by dot blot analysis (Figure S4C). Cluster 5 ("diff.," Figure 2F) represented a subset of day 9 cells with markers of STB, including the two fusogenic endogenous retroviral elements *ERVW-1* and *ERVFRD-1*[30] (Figure 2H; Table S4). Pseudotime analysis using Slingshot identified 2 possible trajectories, both starting from hPSCs (day 0). Trajectory 1 traced a path through clusters 2 and 3 (D3) toward cluster 5 (D6 and D9). Trajectory 2 traced a path through cluster 3 (D3) toward cluster 4 (D6 and D9). Notably, these trajectories showed an expected progression that corresponded with the original sample time points (Figure S4D).

Next, the integration of our dataset with a single-cell transcriptomic profile of human peri-implantation stage embryos[31] revealed close clustering of the embryonic epiblast with hPSCs (day 0) and embryonic TE cells with day 3, 6, and 9 cells (Figure 2I). Another recent report focused on the first-trimester placenta and derived transcriptomic profiles of its single cells.[32] When compared to our dataset, day 0 (hPSC) samples clustered distinctly from all cell types and day 3, 6, and 9 cells were closest to the main primary trophoblastic cell types, which are villous cytotrophoblast (VCT), syncytiotrophoblast (STB), and extravillous trophoblasts (EVT) (Figure 2J). These data suggest that hPSC-derived TE cells are most similar to the early TE of the human embryo rather than fully developed trophoblastic cell types of the placenta. Altogether, single cell analysis and comparison to published datasets confirmed the molecular identity of our hPSC-derived TE cells.

## Derivation and long-term culture of self-renewing trophoblast stem cell lines

The CTB population in the early human placenta is thought to retain trophoblast stem or progenitor cell characteristics.[1] To establish TSC lines, we first tested a previously developed medium[1] but were not able to establish self-renewing TSC lines from TE cells at D10 as only a few epithelial colonies were generated that showed spontaneous differentiation and ceased to proliferate after a few passages (Figure S5A). Hence, we designed the TE3 medium based on strong WNT pathway activation in combination with other factors and conditions that are

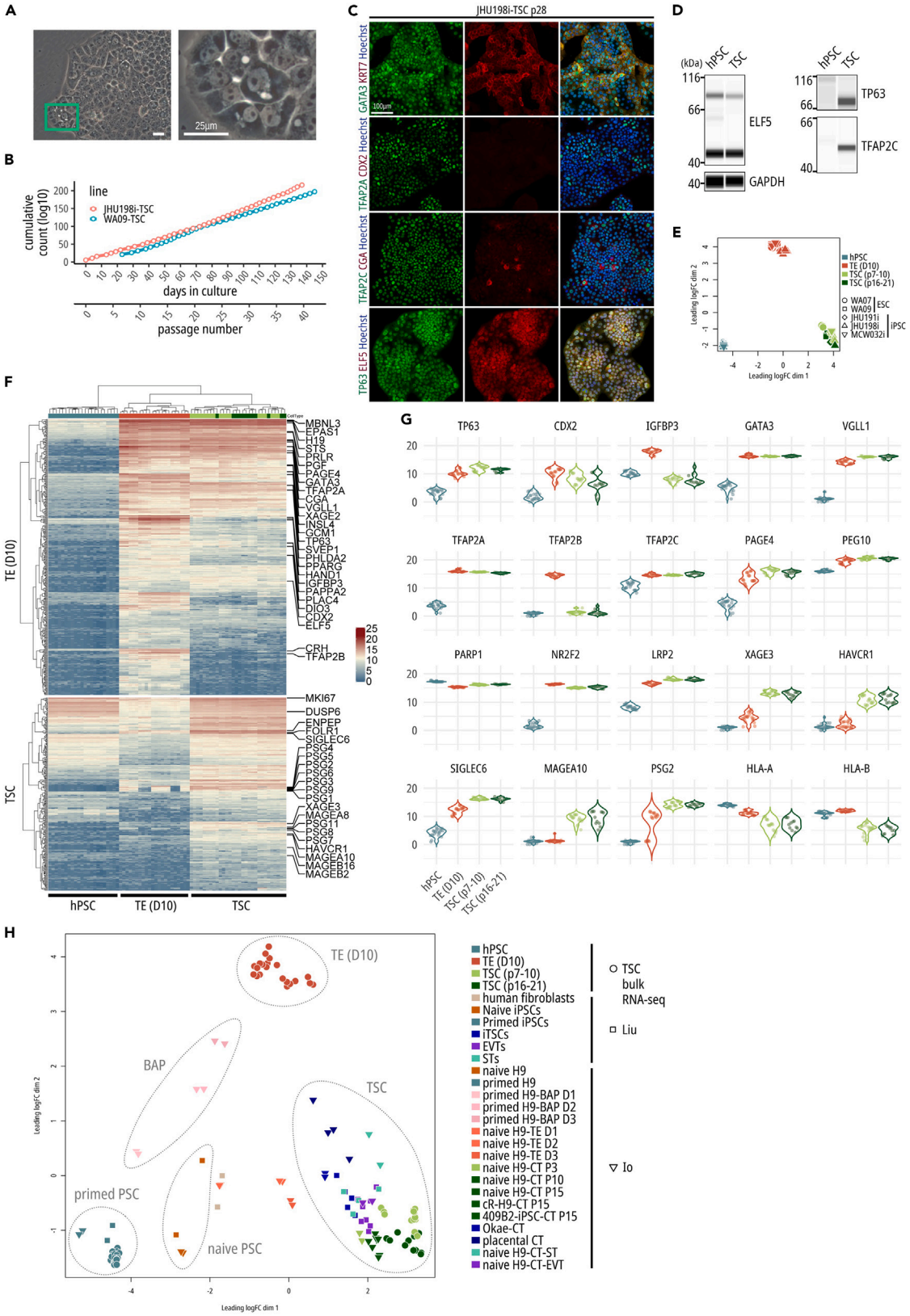
A
25μm
B
line
JHU198i-TSC
WA09-TSC
cumulative count (log10)
days in culture
passage number
C
JHU198i-TSC p28
Hoechst GATA3 KRT7
CDX2 Hoechst TFAP2A
CGA Hoechst TFAP2C
ELF5 Hoechst TP63
100μm
D
(kDa) hPSC TSC
116
66
40
ELF5
GAPDH
TP63
TFAP2C
E
hPSC
TE (D10)
TSC (p7-10)
TSC (p16-21)
WA07 ESC
WA09
JHU191i iPSC
JHU198i
MCW032i
Leading logFC dim 1
Leading logFC dim 2
F
TE (D10)
TSC
MBNL3
EPAS1
H19
STS
PRLR
PGF
PAGE4
GATA3
TFAP2A
CGA
VGLL1
XAGE2
INSL4
GCM1
TP63
SVEP1
PHLDA2
PPARG
HAND1
IGFBP3
PAPPA2
PLAC4
DIO3
CDX2
ELF5
CRH
TFAP2B
MKI67
DUSP6
ENPEP
FOLR1
SIGLEC6
PSG4
PSG5
PSG2
PSG6
PSG3
PSG9
PSG1
XAGE3
MAGEA8
PSG11
PSG8
PSG7
HAVCR1
MAGEA10
MAGEB16
MAGEB2
hPSC
TE (D10)
TSC
G
TP63
CDX2
IGFBP3
GATA3
VGLL1
TFAP2A
TFAP2B
TFAP2C
PAGE4
PEG10
PARP1
NR2F2
LRP2
XAGE3
HAVCR1
SIGLEC6
MAGEA10
PSG2
HLA-A
HLA-B
hPSC
TE (D10)
TSC (p7-10)
TSC (p16-21)
H
TE (D10)
BAP
TSC
primed PSC
naive PSC
Leading logFC dim 1
Leading logFC dim 2
hPSC
TE (D10)
TSC (p7-10)
TSC (p16-21)
human fibroblasts
Naive iPSCs
Primed iPSCs
iTSCs
EVTs
STs
naive H9
primed H9
primed H9-BAP D1
primed H9-BAP D2
primed H9-BAP D3
naive H9-TE D1
naive H9-TE D2
naive H9-TE D3
naive H9-CT P3
naive H9-CT P10
naive H9-CT P15
cR-H9-CT P15
409B2-iPSC-CT P15
Okae-CT
placental CT
naive H9-CT-ST
naive H9-CT-EVT
TSC bulk RNA-seq
Liu
Io

**Figure 3. Establishment of self-renewing TSC lines**

(A) Phase-contrast images of hPSC-derived TSCs cultured in TE3 medium (WA09). Scale bars: 25 μm.

(B) Passage-wise cumulative cell counts show the stable proliferation of two TSC lines derived from one iPSC line (JHU198i) and one ESC line (WA09).

(C) Immunofluorescence showing the expression of TE/trophoblast markers in a TSC line at passage 28 (JHU198i). Scale bar: 100 μm.

(D) Western blot analysis of typical TSC markers (ELF5, TP63, and TFAP2C).

(E) RNA-seq MDS plot showing distinct clustering of hPSC, TE D10, and TSC samples, regardless of their genetic background. Early-passage (7–10) and late-passage (16-21) samples were included.

(F) Heatmap of top differentially expressed genes (nearly 700) in TE D10 compared with hPSC (top, log2 fold change >6, FDR-adjusted $p$ value $<1 \times 10^{-4}$) and in TSC compared with TE D10 (bottom, log2 fold change >3, FDR-adjusted $p$ value $<1 \times 10^{-4}$).

(G) Expression of markers associated with TE and trophoblast.

(H) Bulk RNA-seq integration with external datasets. MDS plot of transcriptional profiles of hPSC, TE (D10), and TSC and previously published iTSC,[22] naive hPSC-derived TSC, and placental TSC.[20] The original external sample group labels were maintained. The H9 ESC line is equivalent to WA09 presented here.

important for placental development[1–3,33,36,37] (Figure 1A). We confirmed the strong expression of receptors for two key growth factors, EGF (*EGFR*) and HGF (*MET*), in TE cells at D10 (Figure S3D). WNT agonist CHIR99021 is toxic at higher concentrations[38] and therefore we included the more potent GSK3-beta inhibitor CHIR98014 as previously validated by using the HotSpot kinase assay.[39] Chroman 1 was recently reported as a more potent and specific ROCK inhibitor than Y-27632[40] and was included in the TE3 medium to prevent the detachment of epithelial cells. Upon the enzymatic dissociation of TE (day 10) and plating of small cell clumps into TE3 medium, colonies with proliferative cells formed and adopted a distinct morphology with prominent nucleoli and dark cytoplasm (Figures 1A and 3A). Serial cell passaging was feasible and allowed the establishment of TSC cultures from two hESC and three hiPSC lines (Figures 3A, 3B, and S5B). Self-renewing TSCs were capable of long-term expansion (over 5 months), and remained undifferentiated, and glycogen deposits found in TE cells (Figure 1B) were also detectable in TSCs (Figure S5C). Immunocytochemical analysis showed expression of canonical trophoblast markers GATA3, KRT7, TFAP2A, TFAP2C, TP63, and ELF5 (Figures 3C, 3D, and S5D). Interestingly, CDX2 was either absent (Figure 3C) or heterogeneously expressed (Figures S5D and S6A) depending on the cell line, suggesting an important role for CDX2 in early TE specification but not in TSCs. Western blot experiments revealed that ELF5 was expressed in pluripotent cells and TSCs, whereas TP63 and TFAP2C were expressed in TSCs only (Figure 3D). Lastly, in contrast to hPSCs that were used as controls, established TSC lines did not express pluripotency markers (Figure S6B) and did not pass the criteria for pluripotency as measured by PluriTest indicating their distinct cell type identity (Figure S6C). Altogether, these data demonstrate the establishment of culture conditions enabling the derivation and characterization of self-renewing human TSCs.

## The transcriptome and methylome of trophoblast stem cells

We performed detailed RNA-seq experiments to characterize TSCs. Parental hPSC lines, their differentiated progeny harvested as TE (D10), and established TSC lines showed distinct clustering in the PCA plot (Figure 3E). The transition from pluripotency to TE (D10) resulted in extensive transcriptomic changes (Figure 3F; Table S5), confirming our earlier analysis (Figures 2A–2E). Further changes were observed when TE (D10) was differentiated in TSCs (Figure 3F). Multiple trophoblast markers were upregulated and expressed in a cell type-specific fashion (Figure 3G). Selective markers of primary first-trimester VCT cells (*PAGE4*, *PEG10*, and *PARP1*)[32] and markers associated with stemness of human TSCs (*NR2F2*, *LRP2*, and *PEG10*)[21] were upregulated or highly expressed in TSC. The top 3 genes with the highest increase in expression in TSC over TE (D10) were *XAGE3*, *HAVCR1*, and *MAGEA10*. Pregnancy-specific glycoproteins were upregulated in TSC as compared to TE (D10) samples. HLA-A and -B were downregulated in TSC compared with TE (D10) and hPSC control (Figure 3G). The lack of HLA-B expression in TSC was confirmed by qRT-PCR in comparison with human dermal fibroblasts and was comparably low in the JEG-3 cell line (Figure S7A). Flow cytometry confirmed the downregulation of HLA-A/B/C in TSC compared with hPSC controls (Figure S7B). This downregulation represents one of the molecular trophoblast criteria.[41] HAVCR1 was recently implicated as a marker of TE and was absent in amnion, while IGFBP3 expression followed the opposite trend.[19] *IGFBP3* was strongly upregulated in TE (D10) and returned to its basal level observed in hPSC upon the establishment of TSC. *SIGLEC6*, a marker of CTB cells in the human chorionic villi at week 5, cultured human placenta-derived TSC, and naive human PSC-derived TSC,[20] was moderate in TE (D10) but high in TSC (Figures 3F and 3G).

A direct comparison and integration of RNA-seq data with previously published datasets[20,22] showed that our hPSC samples (D0) clustered closely with primed hPSCs and distinctly from cells with naive pluripotency (Figure 3H). The TSCs derived with our method clustered closely with all trophoblastic cell types, including TSCs derived from first-trimester placental villi. Primed hPSC treated with the BAP protocol did not cluster with any other samples supporting the notion of incomplete differentiation. Interestingly, regardless of whether TSCs were derived from primed or naive hPSCs, they converged on a phenotype with very similar transcriptomic profiles (Figure 3H). In other words, the TE lineage can be directly generated from hPSCs routinely cultured in E8 medium without the induction of naive pluripotency.

Next, scRNA-seq of TSCs (WA09) identified 4 cell clusters (Figure 4A). The majority of cells expressed *PAGE4*, *PEG10*, *PARP1*, *NR2F2*, and *LRP2*. Trophoblast marker VGLL1[21] was expressed at lower levels in cluster 1, which had an elevated expression of *VIM* and *COL1A2*. *CGA*, *INSL4*, and other STB marker expressions were characteristic of cluster 3 and represented a small subpopulation of cells with a spontaneous propensity toward fusion (Figure 4B). Genes identified as markers of each cluster are summarized in Table S6.

Micro-RNA sequencing (miRNA-seq) revealed distinct clustering of hPSC, TE (D10), and TSC (Figures 4C and S8A) and upregulation of all C19MC miRNAs in TSCs, which is a critical trophoblast criterion,[41] compared with hPSC and TE (D10) controls (Figures 4D and S8B). Similarly, because of its importance as a defining trophoblast feature, we analyzed *ELF5* methylation status as well as the global methylome of the

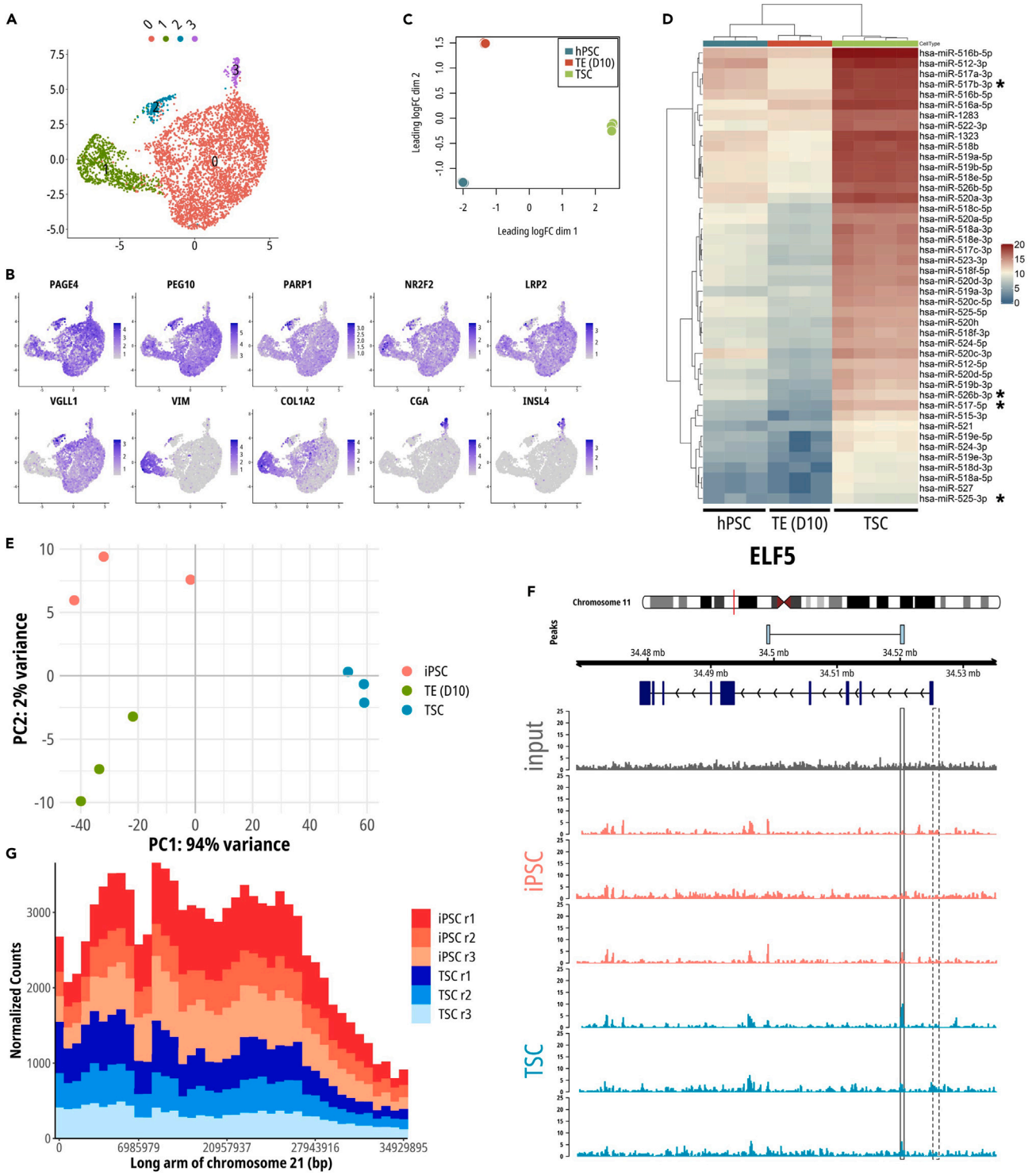


**Figure 4. Single-cell transcriptomics, miRNA expression, and epigenetic analysis of TSCs confirming trophoblast criteria**

(A and B) Single-cell analysis (scRNA-seq) of TSCs (WA09) identified 4 main clusters. Trophoblast markers expressed by CTB of the placental villi and STB.

(C) MDS plot of miRNA expression profiles shows distinct clustering of hPSC, TE (D10), and TSC (JHU198i line).

(D) Heatmap of the expression of microRNAs of the C19MC cluster. The miRNAs marked by asterisks confirm key trophoblast criteria.

(E) Principal component analysis of methylation profiles in iPSCs, TE (D10), and TSC based on MeDIP-seq (JHU198i).

(F) Absence of methylation in the ELF5 promoter region (dashed line) is found across samples.

(G) Low methylation levels along the long arm of chromosome 21 (q21) are consistent with trophoblast identity.

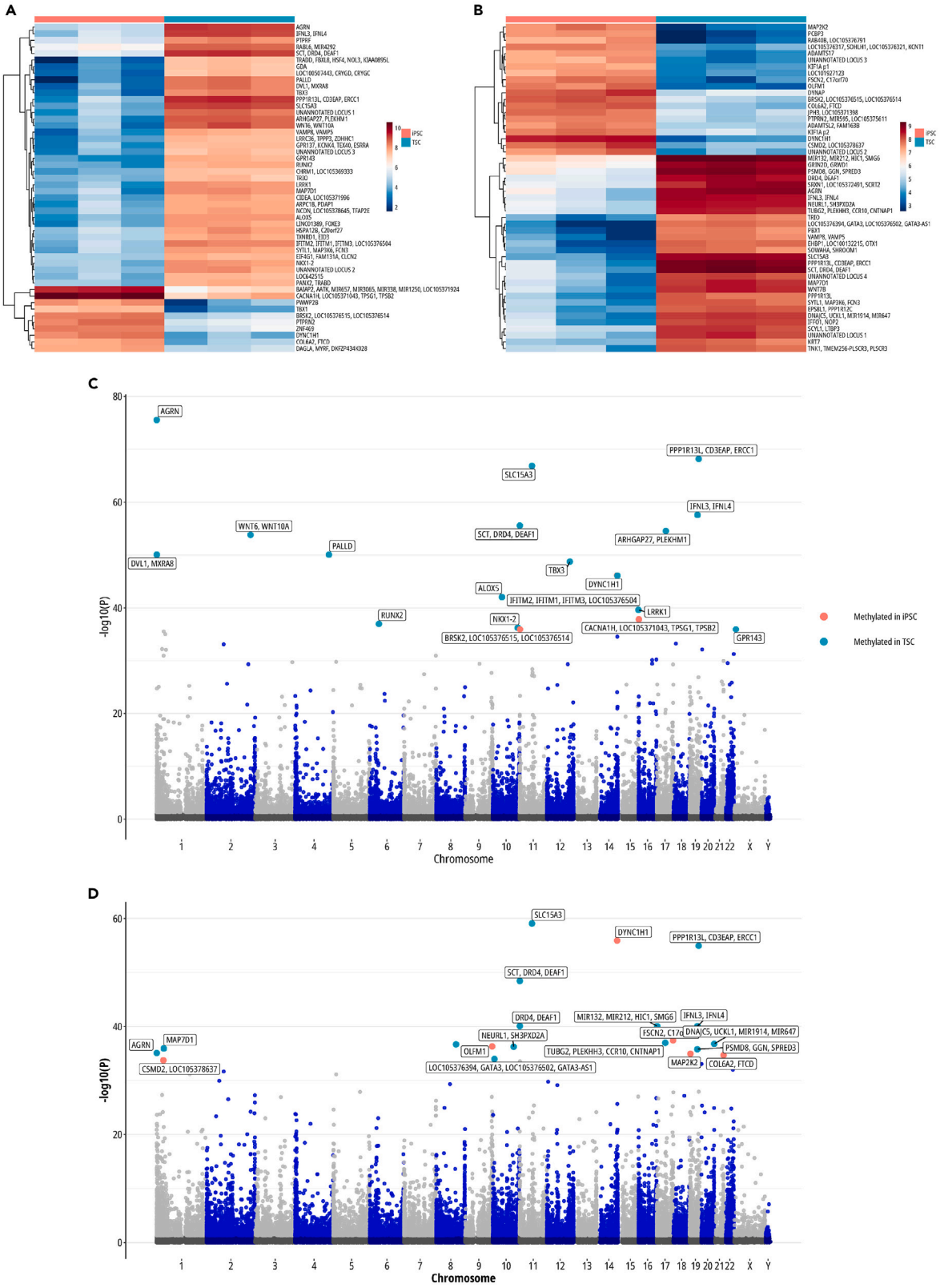
A
B
C
D
-log10(P)
Chromosome
Methylated in iPSC
Methylated in TSC
AGRN
PPP1R13L, CD3EAP, ERCC1
SLC15A3
IFNL3, IFNL4
WNT6, WNT10A
SCT, DRD4, DEAF1
ARHGAP27, PLEKHM1
PALLD
DVL1, MXRA8
TBX3
DYNC1H1
ALOX5
IFITM2, IFITM1, IFITM3, LOC105376504
LRRK1
RUNX2
NKX1-2
CACNA1H, LOC105371043, TPSG1, TPSB2
BRSK2, LOC105376515, LOC105376514
GPR143
DRD4, DEAF1
MIR132, MIR212, HIC1, SMG6
NEURL1, SH3PXD2A
OLFM1
TUBG2, PLEKHH3, CCR10, CNTNAP1
LOC105376394, GATA3, LOC105376502, GATA3-AS1
MAP7D1
CSMD2, LOC105378637
MAP2K2
COL6A2, FTCD
PSMD8, GGN, SPRED3

**Figure 5. MeDIP-seq differential enrichment analysis in TSC**

(A and B) Heatmaps of peaks identified as differentially enriched between human iPSCs and TSCs from two different cell lines. Data in (A) are from JHU198i and data in (B) are from cell lines JHU191i. The peaks are associated with the genes displayed on the heatmap. The colors correspond to the level of methylation, increasing with the values on the color key.

(C and D) Manhattan plots showing peaks that are differentially enriched between iPSC and TSC. The most significant peaks are highlighted and colored based on their methylation either in iPSC or TSC. Data in (C) is from cell line JHU198i and data in (D) is from JHU191i.

hPSC-derived TSCs by using methylated DNA immunoprecipitation sequencing (MeDIP-seq). Undifferentiated iPSCs and TE (D10) showed smaller differences, but the cells underwent dramatic changes in DNA methylation following the establishment of TSCs (Figures 4E and S8C). We, therefore, focused on the comparison of pluripotent cells versus TSCs. The *ELF5* promoter was unmethylated in TSC, which represents one of the trophoblast criteria[41] (Figures 4F and S8D). Notably, unlike previous reports,[3,41] the ELF5 promoter was also unmethylated in hPSC, which may confer TE competency to human cells cultured in chemically defined E8 medium. On the protein level, *ELF5* was expressed in both hPSC and TSC (Figures 3C, 3D, and S5C). On the transcript level, qRT-PCR showed that ELF5 expression in TSC was comparable with JEG-3 and absent in fibroblasts (Figure S7A). Bulk RNA-seq showed its expression in TE (D10) cells as well at a level comparable to CC lines (Figure S7C) and maintained in TSC (Figure S7D).

TSCs were previously reported to have lower levels of methylation along the long arm of chromosome 21.[1,42] We confirmed this feature in hPSC-derived TSCs (Figures 4G and S8E). The MeDIP-seq global methylation changes were summarized for further analysis in the form of heatmaps (Figures 5A and 5B) and Manhattan plots (Figures 5C and 5D) of the most highly differentially enriched peaks (Table S7) and locus plots of the top 8 differentially methylated genes (Figures 6A and 6B). Using our bulk RNA-seq data, we also compared the expression of methyltransferases (DNMT3A, DNMT3B, DNNT1) and demethylases (TET1, TET2, TET3) in hPSCs, differentiating cells (embryonic germ layers, TE and TSC), and CC lines (Figures S7E and S7F). In comparison to hPSCs, only TET2 showed a modest increase in expression in TE and TSC (Figure S7F). In summary, analysis of gene and miRNA expression and methylation status of ELF5 and the long arm of chromosome 21 confirmed the molecular identity of human TSCs and established rich datasets for future data mining.

### Differentiation of trophoblast stem cells into terminal cell types

To differentiate TSCs into STB, we treated cells with forskolin[1] and the ROCK kinase inhibitor Chroman 1[40] (Figure 7A). Over the course of differentiation, multinucleated cells formed and expressed STB markers CGA and DAB2 (Figure 7B). ZO-1 expression disappeared between the individual cells upon fusion, whereas TFAP2C remained expressed in both TSC and STB. After 4 days in culture, almost 50% of the nuclei were embedded in multinucleated cells (Figure 7C).

Next, we attempted to apply a previously published method for the differentiation of TSCs into EVT[1] that included NRG1, however, we were unable to reproduce the epithelial-to-mesenchymal transition (EMT) and formation of cells with spindle-shaped morphology. Hence, for efficient EMT induction, we designed a novel EVT medium containing a combination of EGF, NRG1, TGFβ1, and Chroman 1 (Figure 7D). TGFβ1 was included because it is a well-known inducer of EMT,[43] although there are conflicting reports on its role in EVT differentiation.[44] In addition to the EVT medium composition, incubation in hypoxic culture conditions (2% oxygen) was used as it was previously reported to enhance the differentiation of TSC into EVT.[45] When exposed to these conditions, TSCs underwent EMT and acquired spindle-shaped morphologies (Figure 7D). Immunocytochemistry (Figures 7E, S9A, and S9B) and Western blot analysis (Figure 7F) confirmed the expression of the EVT markers in these cells and their absence in hPSC and TSC controls. Hence, the differentiation of TSCs into terminal cell types with distinct molecular and cellular features provided additional evidence for their biological identity.

Next, to optimize cell viability during TSC line expansion, we incorporated the recently developed CEPT small molecule cocktail,[40] which has been shown to have beneficial effects on cell survival and cytoprotection of hPSCs and other cell types. CEPT treatment for 24 h at each passage led to a significant reduction in the proportion of dead cells as measured over multiple passages and compared to the application of the ROCK pathway inhibitor Chroman 1 only (Figures 7G, 7H, and S9C). These observations were replicated in an additional instance of TSC establishment from WA09 (Figure S9D) and two iPSC lines (Figures S9E and S9F). To summarize all results, we propose a defined *in vitro* roadmap for hPSC-derived TE specification and TSC establishment that recapitulates hallmarks of early human placental development (Figure 7I). Furthermore, culture conditions were established that demonstrated efficient differentiation of human TSCs into STB and EVT. These in vitro models offer new opportunities for basic and translational research. For instance, we succesfully infected TSCs with Zika virus (data not shown), which is a viral agent that can lead to complications during pregnancy and cause birth defects such as microcepahly.

## DISCUSSION

Here, we demonstrate that conventional hESC and iPSC lines cultured in E8 medium can be directly and reproducibly differentiated into TE, without the induction of embryonic germ layers, and self-renewing TSCs that can be expanded for several months, cryopreserved, and differentiated into STB and EVT. Extensive molecular and cellular characterization experiments using genetic and epigenetic analyses and comparisons to other cell types and lineages provided strong support for our conclusions and established a rich resource for data mining. We discovered that human placental cells can be routinely derived from hPSCs with relative ease, which is of great importance for scalable experiments and translational studies. Unlike previous reports, our methods are based on using chemically defined conditions while genetic manipulation and induction of naive pluripotency were not necessary.

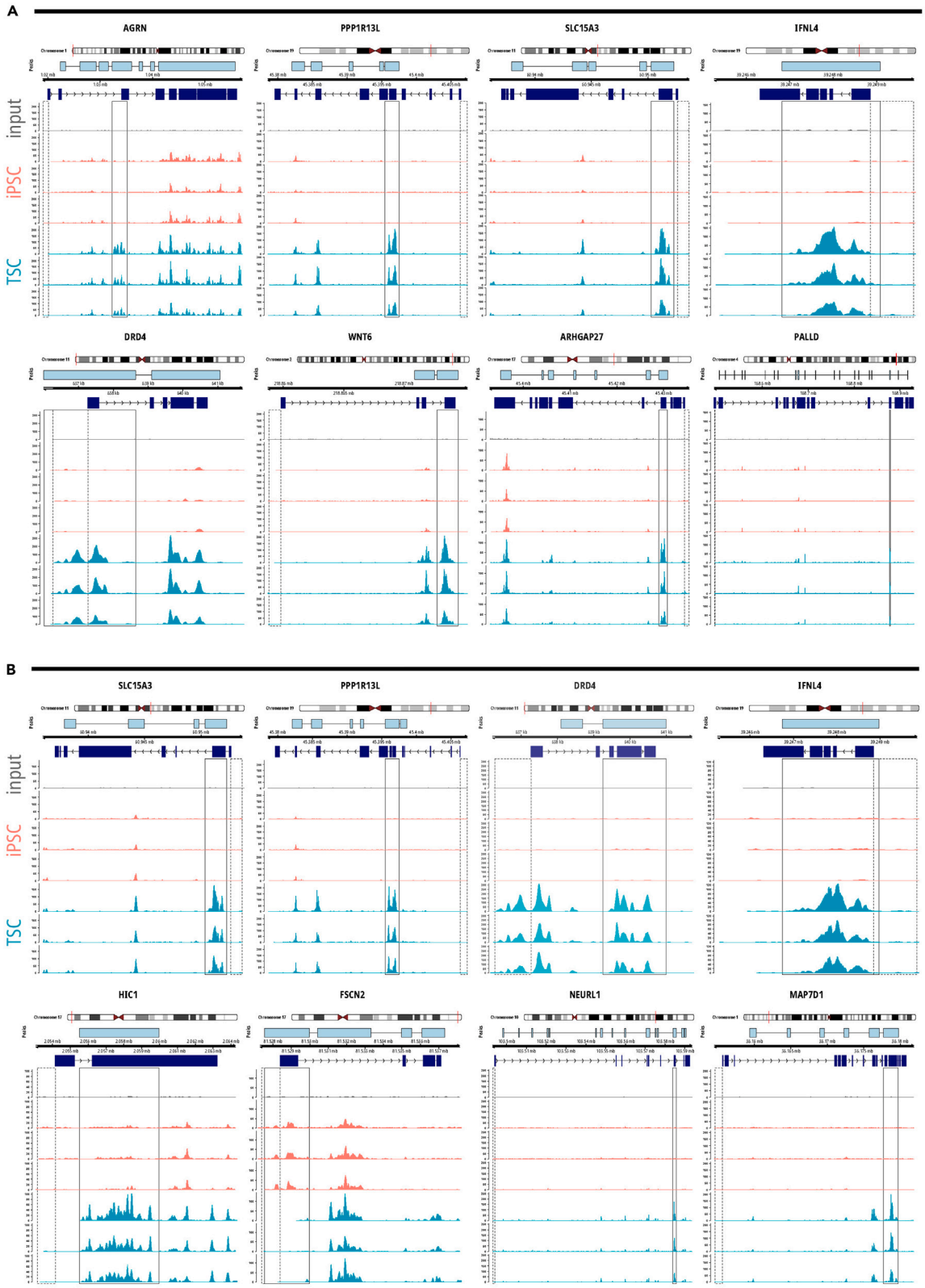
A
AGRN
PPP1R13L
SLC15A3
IFNL4
input
iPSC
TSC
DRD4
WNT6
ARHGAP27
PALLD
B
SLC15A3
PPP1R13L
DRD4
IFNL4
input
iPSC
TSC
HIC1
FSCN2
NEURL1
MAP7D1

**Figure 6. Identification and comparison of differentially methylated genes in iPSC and TSC (MeDIP-seq locus plots of identified peaks)**
(A and B) Presented genes are the most highly differentially methylated between iPSC and TSC generated from JHU198i (A) and JHU191i (B) iPSC lines. Dashed lines denote promoter regions (1000 bp upstream of the TSS). Solid lines denote differentially methylated regions (merged regions), associated with the genes, between iPSC (control) and TSC groups.

The first report suggesting the possibility of TE competency of hESCs by Thomson and colleagues[10] spurred controversy as certain cell culture conditions seem to induce some but not all TE genes and features. Later, it was suggested that only naive hPSCs could be differentiated into self-renewing TSC when using specific culture conditions,[1] whereas primed cells only generated non-self-renewing CTB in response to BMP4 but failed to generate TSCs.[3–5,18,46,47] It was also reported that primed hPSCs may differentiate into amniotic epithelium instead of TE.[19] These observations were replicated in a concurrent study and the resulting TSCs passed the trophoblast criteria, whereas primed hPSCs incompletely differentiated into TE-like cells using the BAP protocol.[20] A more complex approach for deriving human TSCs is to isolate a subpopulation of cells with trophoblast properties that emerged during the reprogramming of fibroblasts into iPSCs.[21,22]

The newly established TSC lines described here displayed typical properties, including terminal differentiation into EVT and STB. However, during the TE differentiation in TE1 and TE2 media, transient activation of an amnion-like program is not ruled out due to the expression of genes such as IGFBP3 or GABRP, similar to what is observed in BAP-treated hPSC.[6,20,48] However, a distinct gene expression pattern in an early amnion in the human embryo has not yet been well-defined due to low numbers of recovered cells.[49] A possibility of misidentification of cell populations in scRNA-seq data was raised as well.[6] Additionally, amnion and trophoblast likely share the expression of multiple genes and this overlap does not preclude trophoblast identity in hPSC-derived TE and TSCs. Indeed, re-analysis of previously published RNA-seq datasets pointed to the trophoblast nature of BAP-treated hPSCs rather than amnion.[11] The established proliferative TSC, however, did not display amnion-related gene expression. Defining new markers and elucidating the mechanism of the establishment of TSCs from primed hPSC will be of interest in future studies to answer questions about whether a common progenitor to TE and amnion could exist or whether a nascent amnion is capable of transdifferentiating into the trophoblast lineage[49] or simply that several amnion-related genes are transiently activated during TE differentiation.[50] Recently, the derivation of TSCs from primed hPSCs was reported by others,[3,4] further supporting the notion that naive pluripotency is dispensable for generating extra-embryonic tissues. Naive hPSC could even be less suitable for this purpose given their global methylation erasure, compromising their use for disease modeling.[47] Furthermore, our findings highlight the broader developmental plasticity of primed hPSCs when cultured *in vitro*[51] and it is important to note that our understanding of different pluripotency states continues to evolve. Interestingly, it was reported that culturing hPSCs in lipid-free E8 medium leads to complex metabolic and epigenetic changes, including a lower level of methylated CpC islands in promoter regions.[52] The authors concluded that hPSCs cultured in E8 medium acquire a distinct intermediate pluripotency state as compared to primed and naive pluripotency,[52] which may explain the efficient trophectoderm differentiation reported in our study.

In summary, we envisage that the detailed characterization experiments and rich datasets presented here will serve as an invaluable resource for studying the lineage commitment of embryonic and extra-embryonic tissues. Most importantly, our study provides the framework for utilizing human placental cells from an inexhaustible source such as iPSCs for better understanding and treating infertility and gestational diseases.

### Limitations of the study

Determining the similarity of the hPSC-derived TSC lines with human embryos and primary fetal tissues was not possible due to NIH policies. Instead, we relied on the integration of RNA-seq datasets from the published literature. The chemically defined E8 medium seemed to result in a unique methylation profile, which warrants future comparative studies considering other widely used media compositions (e.g., KnockOut Serum Replacement, MEF-conditioned medium, mTeSR). In addition, a comparative analysis of time course methylome changes of differentiating hPSCs was not possible due to the lack of available MeDIP-seq datasets of a similar experimental design.

## RESOURCE AVAILABILITY

### Lead contact

Further information and requests about this study should be directed to and will be fulfilled by the lead contact, Ilyas Singeç (ilyassingec@gmail.com), in coordination with team members.

### Materials availability

This study did not generate new unique reagents.

### Data and code availability

- All sequencing data was deposited to the NCBI Short Read Archive (SRA) under accession BioProject: PRJNA760795. This data is publicly available. Accession number is also listed in the key resources table. Previously published datasets used in this study were: BioProject: PRJNA431392, BioProject: PRJNA492902, BioProject: PRJNA605646, BioProject: PRJNA632917, also listed in the key resources table.
- Analysis code is available at https://github.com/cemalley/Slamecka_methods.git.
- Any additional information required to reanalyze the data reported in this article is available from the lead contact.

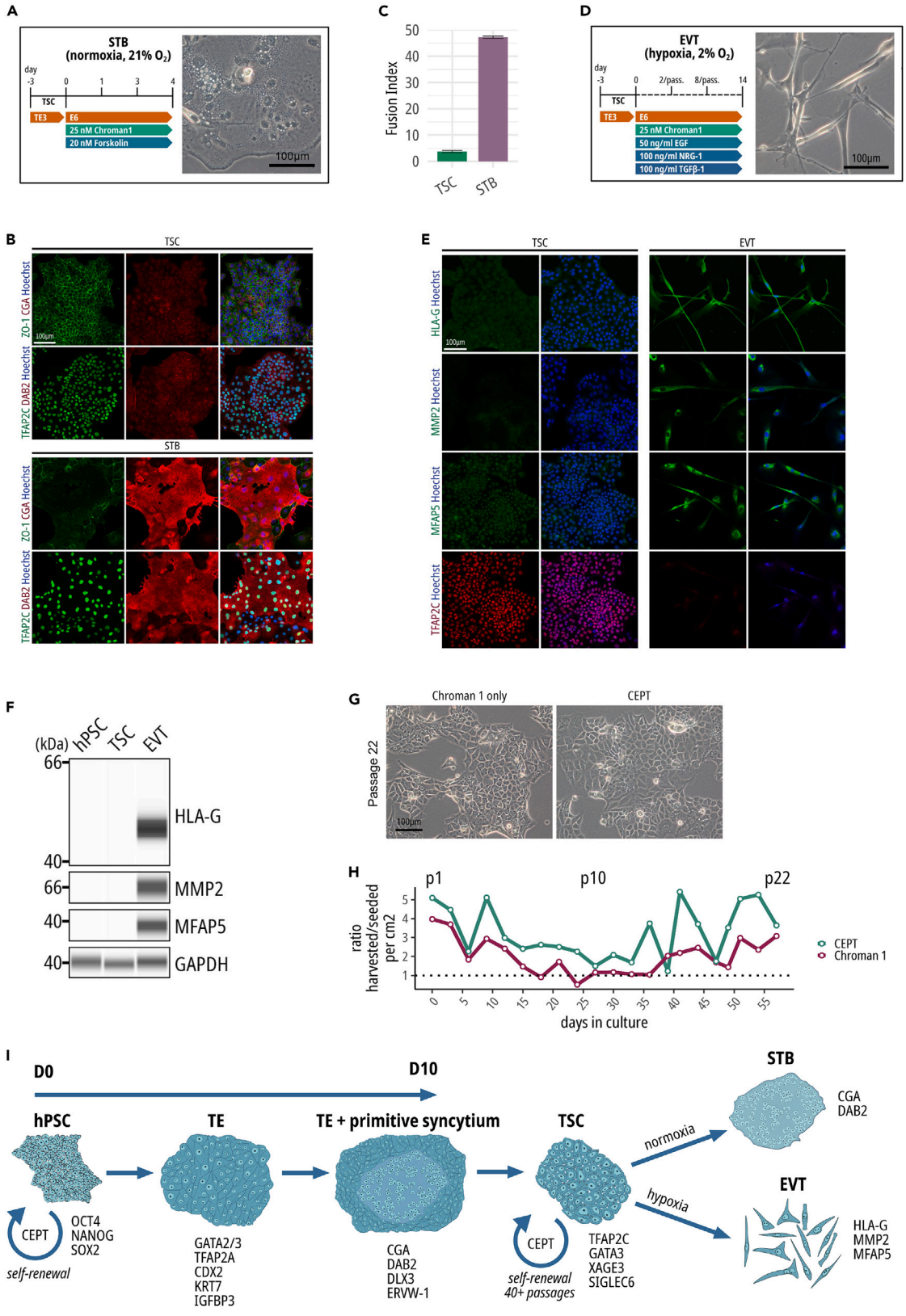
A
STB
(normoxia, 21% O2)
day
-3
0
1
3
4
TSC
TE3
E6
25 nM Chroman1
20 nM Forskolin
100µm
C
Fusion Index
50
40
30
20
10
0
TSC
STB
D
EVT
(hypoxia, 2% O2)
day
-3
0
2/pass.
8/pass.
14
TSC
TE3
E6
25 nM Chroman1
50 ng/ml EGF
100 ng/ml NRG-1
100 ng/ml TGFβ-1
100µm
B
TSC
ZO-1 CGA Hoechst
TFAP2C DAB2 Hoechst
100µm
STB
ZO-1 CGA Hoechst
TFAP2C DAB2 Hoechst
E
TSC
EVT
HLA-G Hoechst
100µm
MMP2 Hoechst
MFAP5 Hoechst
TFAP2C Hoechst
F
(kDa)
hPSC
TSC
EVT
66
HLA-G
40
66
MMP2
40
MFAP5
40
GAPDH
G
Chroman 1 only
CEPT
Passage 22
100µm
H
p1
p10
p22
ratio harvested/seeded per cm2
5
4
3
2
1
0
5
10
15
20
25
30
35
40
45
50
55
days in culture
CEPT
Chroman 1
I
D0
D10
hPSC
TE
TE + primitive syncytium
TSC
STB
normoxia
CGA
DAB2
hypoxia
EVT
HLA-G
MMP2
MFAP5
CEPT
OCT4
NANOG
SOX2
self-renewal
GATA2/3
TFAP2A
CDX2
KRT7
IGFBP3
CGA
DAB2
DLX3
ERVW-1
CEPT
TFAP2C
GATA3
XAGE3
SIGLEC6
self-renewal
40+ passages

**Figure 7. Terminal differentiation of TSCs and improved TSC expansion by using the CEPT cocktail**

(A) Protocol for the differentiation of TSC into STB over roughly 4 days, leading to the formation of multinucleated cells. Scale bar: 100 μm.

(B) Immunofluorescence of STB markers CGA and DAB2, TSC marker TFAP2C, and gap junction protein ZO-1 (GJP1) delineating cellular borders. Scale bar: 100 μm

(C) Fusion index, which is the proportion of nuclei in multinucleated STB cells relative to all nuclei, was calculated from the fluorescent images.

(D) Protocol for the differentiation of TSC into EVT over 14 days with passaging ("pass.") on days 2 and 8, and typical cell morphology. Scale bar: 100 μm

(E) Immunofluorescence analysis of EVT markers after the directed differentiation of TSCs into EVT (WA09). Scale bar: 100 μm.

(F) Western blot analysis of specific markers expressed by hPSC, TSC, and EVT (WA09).

(G) Representative phase-contrast images of TSC lines derived using CEPT compared to control (Chroman 1 only). Scale bar: 100 μm.

(H) Ratio of the number of harvested cells per $cm^2$ divided by the number of seeded cells per $cm^2$ at each passage, in CEPT-treated and control (Chroman 1 only) TSC.

(I) Summary of placental cell development recapitulated by the directed differentiation of hPSCs into distinct cell types expressing specific markers and showing distinct morphologies. The use of the CEPT small molecule cocktail is recommended at the indicated steps.

## ACKNOWLEDGMENTS

We thank all our colleagues at NIH for their contributions. This work utilized the computational resources of the NIH HPC Biowulf cluster (http://hpc.nih.gov). MeDIP-seq analysis and single-cell data integration was completed in part by Rancho Biosciences. Graphic illustrations were designed by the NIH Medical Arts Branch. The authors also thank Hannah Baskir for editing an earlier version of this article. This study was supported by the NIH Common Fund (Regenerative Medicine Program) and the Intramural Research Program of the National Center for Advancing Translational Sciences. The funders had no role in study design, data collection, and analysis; decision to publish or preparation of the article.

## AUTHOR CONTRIBUTIONS

J.S. and I.S. conceived and led the project. Experiments: J.S., S.R., C.A.T., T.D., Y.G., and P.O. Data analysis and discussions: J.S., C.A.T., S.R., P-H.C., T.D., Y.G., P.O., S.M., T.C.V., A.S., and I.S. Manuscript writing: J.S. and I.S.

## DECLARATION OF INTERESTS

J.S., T.D., A.S., and I.S. are co-inventors on a US Department of Health and Human Services patent application covering the trophectoderm/trophoblast differentiation method and its utilization.

## STAR★METHODS

Detailed methods are provided in the online version of this paper and include the following:

- KEY RESOURCES TABLE
- EXPERIMENTAL MODEL AND STUDY PARTICIPANT DETAILS
  - Cell lines and culture
- METHOD DETAILS
  - Differentiation of hPSCs into TE and TSC
  - Differentiation of TSCs into EVT and STB
  - Differentiation of hPSC into ectoderm, mesoderm, and endoderm
  - Cryopreservation
  - Immunocytochemistry
  - Calcein AM and propidium iodide staining
  - Periodic Acid-Schiff (PAS) staining
  - High-content imaging
  - Time-lapse video microscopy
  - Transmission electron microscopy
  - Flow cytometry
  - Western blot
  - qRT-PCR
  - Bulk RNA-seq
  - PluriTest
  - scRNA-seq
  - miRNA-seq
  - MeDIP-seq
  - Pregnancy test
  - Secretome analysis
- QUANTIFICATION AND STATISTICAL ANALYSIS

## SUPPLEMENTAL INFORMATION

Supplemental information can be found online at https://doi.org/10.1016/j.isci.2024.110874.

Received: December 18, 2023
Revised: June 2, 2024
Accepted: August 30, 2024
Published: September 3, 2024

## SUPPORTING CITATIONS

The following references appear in the Supplemental Information: [53–81].

## REFERENCES


1. Okae, H., Toh, H., Sato, T., Hiura, H., Takahashi, S., Shirane, K., Kabayama, Y., Suyama, M., Sasaki, H., and Arima, T. (2018). Derivation of Human Trophoblast Stem Cells. Cell Stem Cell *22*, 50–63.e6. https://doi.org/10.1016/j.stem.2017.11.004.
2. Turco, M.Y., Gardner, L., Kay, R.G., Hamilton, R.S., Prater, M., Hollinshead, M.S., Mcwhinnie, A., Esposito, L., Fernando, R., Skelton, H., et al. (2018). Trophoblast organoids as a model for maternal–fetal interactions during human placentation. Nature *564*, 263–267. https://doi.org/10.1038/s41586-018-0753-3.
3. Soncin, F., Morey, R., Bui, T., Requena, D.F., Cheung, V.C., Kallol, S., Kittle, R., Jackson, M.G., Farah, O., Chousal, J., et al. (2022). Derivation of functional trophoblast stem cells from primed human pluripotent stem cells. Stem Cell Rep. *17*, 1303–1317. https://doi.org/10.1016/j.stemcr.2022.04.013.
4. Viukov, S., Shani, T., Bayerl, J., Aguilera-Castrejon, A., Oldak, B., Sheban, D., Tarazi, S., Stelzer, Y., Hanna, J.H., and Novershtern, N. (2022). Human primed and naïve PSCs are both able to differentiate into trophoblast stem cells. Stem Cell Rep. *17*, 2484–2500. https://doi.org/10.1016/j.stemcr.2022.09.008.
5. Wei, Y., Wang, T., Ma, L., Zhang, Y., Zhao, Y., Lye, K., Xiao, L., Chen, C., Wang, Z., Ma, Y., et al. (2021). Efficient derivation of human trophoblast stem cells from primed pluripotent stem cells. Sci. Adv. *7*, eabf4416. https://doi.org/10.1126/sciadv.abf4416.
6. Chhabra, S., and Warmflash, A. (2021). BMP-treated human embryonic stem cells transcriptionally resemble amnion cells in the monkey embryo. Biol. Open *10*, bio058617. https://doi.org/10.1242/bio.058617.
7. Pera, M.F., and Rossant, J. (2021). The exploration of pluripotency space: Charting cell state transitions in peri-implantation development. Cell Stem Cell *28*, 1896–1906. https://doi.org/10.1016/j.stem.2021.10.001.
8. Horii, M., Li, Y., Wakeland, A.K., Pizzo, D.P., Nelson, K.K., Sabatini, K., Laurent, L.C., Liu, Y., and Parast, M.M. (2016). Human pluripotent stem cells as a model of trophoblast differentiation in both normal development and disease. Proc. Natl. Acad. Sci. USA *113*, E3882–E3891. https://doi.org/10.1073/pnas.1604747113.
9. Krendl, C., Shaposhnikov, D., Rishko, V., Ori, C., Ziegenhain, C., Sass, S., Simon, L., Müller, N.S., Straub, T., Brooks, K.E., et al. (2017). GATA2/3-TFAP2A/C transcription factor network couples human pluripotent stem cell differentiation to trophectoderm with repression of pluripotency. Proc. Natl. Acad. Sci. USA *114*, E9579–E9588. https://doi.org/10.1073/pnas.1708341114.
10. Xu, R.-H., Chen, X., Li, D.S., Li, R., Addicks, G.C., Glennon, C., Zwaka, T.P., and Thomson, J.A. (2002). BMP4 initiates human embryonic stem cell differentiation to trophoblast. Nat. Biotechnol. *20*, 1261–1264. https://doi.org/10.1038/nbt761.
11. Seetharam, A.S., Vu, H.T.H., Choi, S., Khan, T., Sheridan, M.A., Ezashi, T., Roberts, R.M., and Tuteja, G. (2022). The product of BMP-directed differentiation protocols for human primed pluripotent stem cells is placental trophoblast and not amnion. Stem Cell Rep. *17*, 1289–1302. https://doi.org/10.1016/j.stemcr.2022.04.014.
12. Amita, M., Adachi, K., Alexenko, A.P., Sinha, S., Schust, D.J., Schulz, L.C., Roberts, R.M., and Ezashi, T. (2013). Complete and unidirectional conversion of human embryonic stem cells to trophoblast by BMP4. Proc. Natl. Acad. Sci. USA *110*, E1212–E1221. https://doi.org/10.1073/pnas.1303094110.
13. Sudheer, S., Bhushan, R., Fauler, B., Lehrach, H., and Adjaye, J. (2012). FGF inhibition directs BMP4-mediated differentiation of human embryonic stem cells to syncytiotrophoblast. Stem Cells Dev. *21*, 2987–3000. https://doi.org/10.1089/scd.2012.0099.
14. Bernardo, A.S., Faial, T., Gardner, L., Niakan, K.K., Ortmann, D., Senner, C.E., Callery, E.M., Trotter, M.W., Hemberger, M., Smith, J.C., et al. (2011). BRACHYURY and CDX2 mediate BMP-induced differentiation of human and mouse pluripotent stem cells into embryonic and extraembryonic lineages. Cell Stem Cell *9*, 144–155. https://doi.org/10.1016/j.stem.2011.06.015.
15. Hemberger, M., Udayashankar, R., Tesar, P., Moore, H., and Burton, G.J. (2010). ELF5-enforced transcriptional networks define an epigenetically regulated trophoblast stem cell compartment in the human placenta. Hum. Mol. Genet. *19*, 2456–2467. https://doi.org/10.1093/hmg/ddq128.
16. Lee, C.Q.E., Gardner, L., Turco, M., Zhao, N., Murray, M.J., Coleman, N., Rossant, J., Hemberger, M., and Moffett, A. (2016). Stem Cell Reports. Stem Cell Rep. *6*, 257–272. https://doi.org/10.1016/j.stemcr.2016.01.006.
17. Cinkornpumin, J.K., Kwon, S.Y., Guo, Y., Hossain, I., Sirois, J., Russett, C.S., Tseng, H.W., Okae, H., Arima, T., Duchaine, T.F., et al. (2020). Naive Human Embryonic Stem Cells Can Give Rise to Cells with a Trophoblast-like Transcriptome and Methylome. Stem Cell Rep. *15*, 198–213. https://doi.org/10.1016/j.stemcr.2020.06.003.
18. Dong, C., Beltcheva, M., Gontarz, P., Zhang, B., Popli, P., Fischer, L.A., Khan, S.A., Park, K.M., Yoon, E.J., Xing, X., et al. (2020). Derivation of trophoblast stem cells from naïve human pluripotent stem cells. Elife *9*, e52504. https://doi.org/10.7554/eLife.52504.
19. Guo, G., Stirparo, G.G., Strawbridge, S.E., Spindlow, D., Yang, J., Clarke, J., Dattani, A., Yanagida, A., Li, M.A., Myers, S., et al. (2021). Human naive epiblast cells possess unrestricted lineage potential. Cell Stem Cell *28*, 1040–1056.e6. https://doi.org/10.1016/j.stem.2021.02.025.
20. Io, S., Kabata, M., Iemura, Y., Semi, K., Morone, N., Minagawa, A., Wang, B., Okamoto, I., Nakamura, T., Kojima, Y., et al. (2021). Capturing human trophoblast development with naive pluripotent stem cells *in vitro*. Cell Stem Cell *28*, 1023–1039.e13. https://doi.org/10.1016/j.stem.2021.03.013.
21. Castel, G., Meistermann, D., Bretin, B., Firmin, J., Blin, J., Loubersac, S., Bruneau, A., Chevolleau, S., Kilens, S., Chariau, C., et al. (2020). Induction of Human Trophoblast Stem Cells from Somatic Cells and Pluripotent Stem Cells. Cell Rep. *33*, 108419. https://doi.org/10.1016/j.celrep.2020.108419.
22. Liu, X., Ouyang, J.F., Rossello, F.J., Tan, J.P., Davidson, K.C., Valdes, D.S., Schröder, J., Sun, Y.B.Y., Chen, J., Knaupp, A.S., et al. (2020). Reprogramming roadmap reveals route to human induced trophoblast stem cells. Nature *586*, 101–107. https://doi.org/10.1038/s41586-020-2734-6.
23. Lichtner, B., Knaus, P., Lehrach, H., and Adjaye, J. (2013). BMP10 as a potent inducer of trophoblast differentiation in human embryonic and induced pluripotent stem cells. Biomaterials *34*, 9789–9802. https://doi.org/10.1016/j.biomaterials.2013.08.084.
24. Tunster, S.J., Watson, E.D., Fowden, A.L., and Burton, G.J. (2020). Reproduction Review Placental glycogen stores and fetal growth: insights from genetic mouse models. Reproduction *159*, R213–R235. https://doi.org/10.1530/REP.
25. Deglincerti, A., Croft, G.F., Pietila, L.N., Zernicka-Goetz, M., Siggia, E.D., and Brivanlou, A.H. (2016). Self-organization of the *in vitro* attached human embryo. Nature *533*, 251–254. https://doi.org/10.1038/nature17948.
26. Gunne-Braden, A., Sullivan, A., Gharibi, B., Sheriff, R.S.M., Maity, A., Wang, Y.-F., Edwards, A., Jiang, M., Howell, M., Goldstone, R., et al. (2020). GATA3 Mediates a Fast, Irreversible Commitment to BMP4-Driven Differentiation in Human Embryonic Stem Cells. Cell Stem Cell *26*, 693–706.e9. https://doi.org/10.1016/j.stem.2020.03.005.
27. Rossant, J., and Tam, P.P.L. (2022). Early human embryonic development: Blastocyst formation to gastrulation. Dev. Cell *57*, 152–165. https://doi.org/10.1016/j.devcel.2021.12.022.
28. Karlsson, M., Zhang, C., Méar, L., Zhong, W., Digre, A., Katona, B., Sjöstedt, E., Butler, L., Odeberg, J., Dusart, P., et al. (2021). A single-cell type transcriptomics map of human tissues. Sci. Adv. *7*, eabh2169. https://doi.org/10.1126/sciadv.abh2169.
29. Gerri, C., McCarthy, A., Alanis-Lobato, G., Demtschenko, A., Bruneau, A., Loubersac, S., Fogarty, N.M.E., Hampshire, D., Elder, K., Snell, P., et al. (2020). Initiation of a conserved trophectoderm program in human, cow and mouse embryos. Nature *587*, 443–447. https://doi.org/10.1038/s41586-020-2759-x.
30. Blaise, S., de Parseval, N., Bénit, L., and Heidmann, T. (2003). Genomewide screening for fusogenic human endogenous retrovirus envelopes identifies syncytin 2, a gene conserved on primate evolution. Proc. Natl. Acad. Sci. USA *100*, 13013–13018. https://doi.org/10.1073/pnas.2132646100.
31. Zhou, F., Wang, R., Yuan, P., Ren, Y., Mao, Y., Li, R., Lian, Y., Li, J., Wen, L., Yan, L., et al. (2019). Reconstituting the transcriptome and DNA methylome landscapes of human implantation. Nature *572*, 660–664. https://doi.org/10.1038/s41586-019-1500-0.

32. Suryawanshi, H., Morozov, P., Straus, A., Sahasrabudhe, N., Max, K.E.A., Garzia, A., Kustagi, M., Tuschl, T., and Williams, Z. (2018). A single-cell survey of the human first-trimester placenta and decidua. Sci. Adv. *4*, eaau4788.
33. Thul, P.J., Åkesson, L., Wiking, M., Mahdessian, D., Geladaki, A., Ait Blal, H., Alm, T., Asplund, A., Björk, L., Breckels, L.M., et al. (2017). A subcellular map of the human proteome. Science *356*, eaal3321. https://doi.org/10.1126/science.aal3321.
34. Uhlén, M., Fagerberg, L., Hallstrom, B.M., Lindskog, C., Oksvold, P., Mardinoglu, A., Sivertsson, A., Kampf, C., Sjostedt, E., Asplund, A., et al. (2015). Tissue-based map of the human proteome. Science *347*, 1260419. https://doi.org/10.1126/science.1260419.
35. Uhlen, M., Zhang, C., Lee, S., Sjöstedt, E., Fagerberg, L., Bidkhori, G., Benfeitas, R., Arif, M., Liu, Z., Edfors, F., et al. (2017). A pathology atlas of the human cancer transcriptome. Science *357*, eaan2507. https://doi.org/10.1126/science.aan2507.
36. Haider, S., Meinhardt, G., Saleh, L., Kunihs, V., Gamperl, M., Kaindl, U., Ellinger, A., Burkard, T.R., Fiala, C., Pollheimer, J., et al. (2018). Self-Renewing Trophoblast Organoids Recapitulate the Developmental Program of the Early Human Placenta. Stem Cell Rep. *11*, 537–551. https://doi.org/10.1016/j.stemcr.2018.07.004.
37. Kim, K.-A., Wagle, M., Tran, K., Zhan, X., Dixon, M.A., Liu, S., Gros, D., Korver, W., Yonkovich, S., Tomasevic, N., et al. (2008). R-Spondin family members regulate the Wnt pathway by a common mechanism. Mol. Biol. Cell *19*, 2588–2596. https://doi.org/10.1091/mbc.e08-02-0187.
38. Laco, F., Woo, T.L., Zhong, Q., Szmyd, R., Ting, S., Khan, F.J., Chai, C.L.L., Reuveny, S., Chen, A., and Oh, S. (2018). Unraveling the Inconsistencies of Cardiac Differentiation Efficiency Induced by the GSK3β Inhibitor CHIR99021 in Human Pluripotent Stem Cells. Stem Cell Rep. *10*, 1851–1866. https://doi.org/10.1016/j.stemcr.2018.03.023.
39. Deng, T., Jovanovic, V.M., Tristan, C.A., Weber, C., Chu, P.H., Inman, J., Ryu, S., Jethmalani, Y., Ferreira de Sousa, J., Ormanoglu, P., et al. (2023). Scalable generation of sensory neurons from human pluripotent stem cells. Stem Cell Rep. *18*, 1030–1047. https://doi.org/10.1016/j.stemcr.2023.03.006.
40. Chen, Y., Tristan, C.A., Chen, L., Jovanovic, V.M., Malley, C., Chu, P.H., Ryu, S., Deng, T., Ormanoglu, P., Tao, D., et al. (2021). A versatile polypharmacology platform promotes cytoprotection and viability of human pluripotent and differentiated cells. Nat. Methods *18*, 528–541. https://doi.org/10.1038/s41592-021-01126-2.
41. Lee, C.Q.E., Gardner, L., Turco, M., Zhao, N., Murray, M.J., Coleman, N., Rossant, J., Hemberger, M., and Moffett, A. (2016). What Is Trophoblast? A Combination of Criteria Define Human First-Trimester Trophoblast. Stem Cell Rep. *6*, 257–272. https://doi.org/10.1016/j.stemcr.2016.01.006.
42. Schroeder, D.I., Blair, J.D., Lott, P., Yu, H.O.K., Hong, D., Crary, F., Ashwood, P., Walker, C., Korf, I., Robinson, W.P., and LaSalle, J.M. (2013). The human placenta methylome. Proc. Natl. Acad. Sci. USA *110*, 6037–6042. https://doi.org/10.1073/pnas.1215145110.
43. Xu, J., Lamouille, S., and Derynck, R. (2009). TGF-beta-induced epithelial to mesenchymal transition. Cell Res. *19*, 156–172. https://doi.org/10.1038/cr.2009.5.
44. Pollheimer, J., Vondra, S., Baltayeva, J., Beristain, A.G., and Knöfler, M. (2018). Regulation of Placental Extravillous Trophoblasts by the Maternal Uterine Environment. Front. Immunol. *9*, 2597. https://doi.org/10.3389/fimmu.2018.02597.
45. Wakeland, A.K., Soncin, F., Moretto-Zita, M., Chang, C.-W., Horii, M., Pizzo, D., Nelson, K.K., Laurent, L.C., and Parast, M.M. (2017). Hypoxia Directs Human Extravillous Trophoblast Differentiation in a Hypoxia-Inducible Factor-Dependent Manner. Am. J. Pathol. *187*, 767–780. https://doi.org/10.1016/j.ajpath.2016.11.018.
46. Mischler, A., Karakis, V., San Miguel, A., and Rao, B. (2019). Derivation of human trophoblast stem cells from human pluripotent stem cells. Placenta *83*, e59. https://doi.org/10.1016/j.placenta.2019.06.193.
47. Morey, R., Bui, T., Cheung, V.C., Dong, C., Zemke, J.E., Requena, D., Arora, H., Jackson, M.G., Pizzo, D., Theunissen, T.W., and Horii, M. (2024). iPSC-based modeling of preeclampsia identifies epigenetic defects in extravillous trophoblast differentiation. iScience *27*, 109569. https://doi.org/10.1016/j.isci.2024.109569.
48. Ohgushi, M., Taniyama, N., Vandenbon, A., and Eiraku, M. (2022). Delamination of trophoblast-like syncytia from the amniotic ectodermal analogue in human primed embryonic stem cell-based differentiation model. Cell Rep. *39*, 110973. https://doi.org/10.1016/j.celrep.2022.110973.
49. Roberts, R.M., Ezashi, T., Temple, J., Owen, J.R., Soncin, F., and Parast, M.M. (2022). The Role of BMP4 Signaling in Trophoblast Emergence from Pluripotency (Springer Science and Business Media Deutschland GmbH). https://doi.org/10.1007/s00018-022-04478-w.
50. Karvas, R.M., David, L., and Theunissen, T.W. (2022). Accessing the human trophoblast stem cell state from pluripotent and somatic cells. Cell. Mol. Life Sci. *79*, 604. https://doi.org/10.1007/s00018-022-04549-y.
51. Pera, M.F. (2022). Pluripotent Cell States and Unexpected Fates (Cell Press). https://doi.org/10.1016/j.stemcr.2022.05.011.
52. Cornacchia, D., Zhang, C., Zimmer, B., Chung, S.Y., Fan, Y., Soliman, M.A., Tchieu, J., Chambers, S.M., Shah, H., Paull, D., et al. (2019). Lipid Deprivation Induces a Stable, Naive-to-Primed Intermediate State of Pluripotency in Human PSCs. Cell Stem Cell *25*, 120–136.e10. https://doi.org/10.1016/j.stem.2019.05.001.

## STAR★METHODS

### KEY RESOURCES TABLE

| REAGENT or RESOURCE | SOURCE | IDENTIFIER |
|---|---|---|
| Antibodies | | |
| Purified Mouse anti-Oct3/4 (Human Isoform A) | BD Biosciences | Cat# 561555; RRID: AB_10715577 |
| Purified Mouse anti-Human Nanog | BD Biosciences | Cat# 560482: RRID: AB_1645598 |
| Cytokeratin 18 Antibody | Santa Cruz | sc-6259 |
| AP-2α Antibody (TFAP2A) | Santa Cruz | sc-25343 |
| Anti-CGA Antibody | Atlas Antibodies | HPA029698 |
| Purified anti-human Cytokeratin 7 Antibody | BioLegend | Cat# 601602; RRID: AB_2715905 |
| Anti-TEAD3 Antibody | Atlas Antibodies | HPA028906 |
| Anti-DAB2 Antibody | Atlas Antibodies | HPA028888 |
| Purified Mouse Anti-Human CD324 (E-Cadherin) | BD Biosciences | Cat# 562869; RRID: AB_2737853 |
| CDX2 (D11D10) Rabbit mAb | Cell Signaling Technology | 12306S |
| ZO-1 Monoclonal Antibody (ZO1-1A12) | Thermo-Fisher | Cat # 33-9100; RRID: AB_2533147 |
| ELF5 Polyclonal Antibody | Thermo-Fisher | Cat# 720380: RRID: AB_2688046 |
| AP-2γ Antibody (6E4/4) (TFAP2C) | Santa Cruz | sc-12762 |
| p63 Antibody (D-9) | Santa Cruz | sc-25268 |
| Brachyury Antibody | Novus/R&D | NBP1-87598 |
| Purified Mouse anti-GATA3 | BD Biosciences | Cat# 558686; RRID: AB_2108590 |
| Anti-Human IGFBP-3 | BD Biosciences | Cat# 611504; RRID: AB_398964 |
| Monoclonal Anti-YAP1 antibody produced in mouse | Millipore-Sigma | WH0010413M1-100UG |
| Anti-Ki67 antibody (ab15580) | Abcam | ab15580 |
| Zika virus Envelope protein antibody | GeneTex | Cat# GTX133314; RRID: AB_2747413 |
| HLA-G (E8N9C) XP® Rabbit mAb | Cell Signaling Tech | 79769S |
| Anti-HLA-G Antibody, clone 4H84 | Millipore-Sigma | MABF2169-25UG |
| MMP-2 (D4M2N) Rabbit mAb #40994 | Cell Signaling Tech | 40994S |
| Anti-MFAP5 Antibody | Atlas Antibodies | HPA010553 |
| Anti-SIGLEC6 antibody produced in rabbit | Millipore-Sigma | HPA009084-100UL |
| GAPDH Antibody | Santa Cruz | sc-365062 |
| HLA-G (E8N9C) XP® Rabbit mAb | Cell Signaling Tech | 79769S |
| MMP-2 (D4M2N) Rabbit mAb #40994 | Cell Signaling Tech | 40994S |
| Anti-MFAP5 Antibody | Atlas Antibodies | HPA010553 |
| Alexa Fluor® 647 Mouse IgG1, κ Isotype Ctrl (FC) Antibody | BioLegend | Cat# 400130; RRID: AB_2800436 |
| BD Horizon™ BV421 Mouse IgG1, k Isotype Control | BD Biosciences | Cat# 562438; RRID: AB_11207319 |
| PE Mouse IgG2a, κ Isotype Ctrl (FC) Antibody | BioLegend | Cat# 400213; RRID: AB_2800438 |
| Alexa Fluor® 647 anti-human EGFR Antibody | BioLegend | Cat# 352917; RRID: AB_2650983 |
| BD OptiBuild™ BV421 Mouse Anti-Human CD249 | BD Biosciences | Cat# 744872; RRID: AB_2742549 |
| PE anti-human TACSTD2 (TROP2) Antibody | BioLegend | Cat# 363803; RRID: AB_2572021 |
| Mouse IgG2a kappa Isotype Control (eBM2a), FITC, eBioscience™ | ThermoFisher | Cat# 11-4724-82; RRID: AB_470028 |
| HLA-ABC Monoclonal Antibody (W6/32), FITC, eBioscience™ | ThermoFisher | Cat# 11-9983-42; RRID: AB_1633402 |
| Bacterial and virus strains | | |
| Zika virus, strain: MR 766 (Original) | ATCC | VR-84 |
| VERO 76 | ATCC | CRL-1587 |

(*Continued on next page*)

*Continued*

| REAGENT or RESOURCE | SOURCE | IDENTIFIER |
|---|---|---|
| Chemicals, peptides, and recombinant proteins | | |
| Vitronectin (VTN-N) Recombinant Human Protein, Truncated | Thermo Fisher Scientific | A14700 |
| UltraPure™ 0.5M EDTA, pH 8.0 | Thermo Fisher Scientific | 15575020 |
| DPBS, no calcium, no magnesium | Thermo Fisher Scientific | 14190144 |
| A83-01 | Tocris / R&D | 2939 |
| CHIR99021 trihydrochloride | Tocris / R&D | 4953 |
| CH5183284 | SelleckChem | S7665 |
| Recombinant Human BMP-4 Protein | R&D | 314-BP-050 |
| Recombinant Human BMP-10 Protein | R&D | 2926-BP-025 |
| CHIR98014 | Selleck Chem | S2745 |
| Prostaglandin E2 | Tocris / R&D | 2296 |
| Chroman 1 | MedChem | HY-15392 |
| Recombinant Human EGF Protein, CF | R&D | 236-EG-200 |
| Recombinant Human HGF (NS0-expressed) Protein | R&D | 294-HGN-100 |
| Recombinant Human R-Spondin 1 Protein | R&D | 4645-RS-100 |
| Recombinant Human R-Spondin 3 Protein | R&D | 3500-RS-025 |
| Forskolin | Tocris / R&D | 1099 |
| Recombinant Human NRG1/HRG1 Protein, CF | R&D | 5898-NR-050 |
| Recombinant Human TGF-beta 1 (Human Cell-expressed) Protein | R&D | 7754-BH-100 |
| LDN 193189 dihydrochloride | Tocris / R&D | 6053 |
| RIPA Lysis and Extraction Buffer | Thermo Fisher Scientific | 89901 |
| QIAzol Lysis Reagent | Qiagen | 79306 |
| 10 mM Tris-HCl pH 8.5 | Teknova | T1062 |
| Triton™ X-100 Surfact-Amps™ Detergent Solution | Thermo-Fisher | 85111 |
| Bovine Serum Albumin, lyophilized powder, BioReagent, suitable for cell culture | Millipore-Sigma | A9418-100G |
| Pierce™ 16% Formaldehyde (w/v), Methanol-free | Thermo Fisher Scientific | 28908 |
| Methanol, anhydrous, 99.8% | Millipore-Sigma | 322415-100ML |
| Normal Donkey Serum | Jackson ImmunoResearch | 017-000-121 |
| Hoechst 33342 Solution (20 mM) | Thermo Fisher Scientific | 62249 |
| Propidium iodide 1 mg/ml | Alfa Aesar | J66584-AB |
| Ethyl alcohol, Pure, 200 proof, for molecular biology | Millipore-Sigma | E7023 |
| Emricasan | SelleckChem | S7775 |
| Polyamine Supplement (1000×) | Millipore-Sigma | P8483-5ML |
| trans-ISRIB | Tocris / R&D | 5284 |
| Critical commercial assays | | |
| Fibroblast Basal Medium | ATCC | PCS-201-030 |
| Fibroblast Growth Kit-Low serum | ATCC | PCS-201-041 |
| STEMdiff™ Definitive Endoderm Kit (TeSR™-E8™ Optimized) | Stemcell Technologies | 05115 |
| STEMdiff™ Mesoderm Induction Medium | Stemcell Technologies | 05221 |
| High-Capacity RNA-to-cDNA™ Kit | Thermo-Fisher | 4388950 |
| 25 mL PrimeTime® Gene Expression Master Mix | Integrated DNA Technologies | 1055771 |
| cOmplete™, Mini Protease Inhibitor Cocktail | Roche | 04-693-124-001 |
| Pierce™ BCA Protein Assay Kit | Thermo Fisher Scientific | 23225 |
| 12-230 kDa Separation Module, 2 x 25 capillary cartridges, for capillary Western blot by Wes | ProteinSimple | SM-W003 |

(*Continued on next page*)

*Continued*

| REAGENT or RESOURCE | SOURCE | IDENTIFIER |
|---|---|---|
| Anti-Rabbit Detection Module, for capillary Western by Wes | ProteinSimple | DM-001 |
| Anti-Mouse Detection Module, for capillary Western by Wes | ProteinSimple | DM-002 |
| RNeasy Plus Mini Kit (250) | Qiagen | 74136 |
| RNA ScreenTape | Agilent Technologies | 5067-5576 |
| RNA ScreenTape Sample Buffer | Agilent Technologies | 5067-5577 |
| RNA ScreenTape Ladder | Agilent Technologies | 5067-5578 |
| D1000 ScreenTape | Agilent Technologies | 5067-5582 |
| D1000 Reagents (ladder and sample buffer) | Agilent Technologies | 5067-5583 |
| D5000 ScreenTape | Agilent Technologies | 5067-5588 |
| D5000 Reagents (ladder and sample buffer) | Agilent Technologies | 5067-5589 |
| KAPA mRNA HyperPrep Kit | Roche Life Science | KK8581 |
| KAPA Unique Dual-Indexed Adapter Kit, (15 μM) | Roche Life Science | KK8727 |
| KAPA Adapter Dilution Buffer (25 mL) | Roche Life Science | KK8721 |
| KAPA Library Quantification Kit - Complete kit (Universal) | Roche Life Science | KK4824 |
| NovaSeq 6000 S4 Reagent Kit (300 cycles) | Illumina | 20012866 |
| Chromium™ Single Cell 3′ Library & Gel Bead Kit v2, 16 rxns | 10X Genomics | 120237 |
| Chromium™ Single Cell A Chip Kit, 48 rxns | 10X Genomics | 120236 |
| Chromium™ i7 Multiplex Kit, 96 rxns | 10X Genomics | 120262 |
| Chromium™ Single Cell 3′ GEM, Library & Gel Bead Kit v3, 16 rxns | 10X Genomics | 1000075 |
| Chromium™ Chip B Single Cell Kit, 48 rxns | 10X Genomics | 1000073 |
| Calcein AM - LIVE/DEAD™ Viability/Cytotoxicity Kit, for mammalian cells | Thermo Fisher Scientific | L3224 |
| Periodic Acid-Schiff (PAS) Kit | Millipore-Sigma | 395B |
| PrimeTime Std® qPCR Assay, ELF5, Homo_sapiens | Integrated DNA Technologies | Hs.PT.58.133268.g |
| PrimeTime Std® qPCR Assay, GATA3, Homo_sapiens | Integrated DNA Technologies | Hs.PT.58.19431110 |
| PrimeTime Std® qPCR Assay, HLA-B, Homo_sapiens | Integrated DNA Technologies | Hs.PT.58.38856671.g |
| PrimeTime Std® qPCR Assay, TFAP2C, Homo_sapiens | Integrated DNA Technologies | Hs.PT.58.40121112 |
| PrimeTime Std® qPCR Assay, TP63, Homo_sapiens | Integrated DNA Technologies | Hs.PT.58.2966111 |
| PrimeTime Std® qPCR Assay, GAPDH, Homo_sapiens | Integrated DNA Technologies | Hs.PT.39a.22214836 |
| **Deposited data** | | |
| This study, raw sequence files | Sequence Read Archive | BioProject: PRJNA760795 |
| Human embryo scRNA-seq (ref. 34) | Sequence Read Archive | BioProject: PRJNA431392 |
| Placenta scRNA-seq (ref. 35) | Sequence Read Archive | BioProject: PRJNA492902 |
| Naïve hPSC-derived TSC bulk RNA-seq (ref. 20) | Sequence Read Archive | BioProject: PRJNA605646 |
| iTSC bulk RNA-seq (ref. 22) | Sequence Read Archive | BioProject: PRJNA632917 |
| **Experimental models: Cell lines** | | |
| WA09 | WiCell | N/A |
| WA07 | WiCell | N/A |
| WA014 | WiCell | N/A |
| JHU191i | WiCell | N/A |
| JHU198i | WiCell | N/A |
| MCW032i | WiCell | N/A |
| LiPSC-GR1.1 | NIH Common Fund | N/A |
| NCRM5 (NL5) | NIH Common Fund | N/A |
| JEG-3 choriocarcinoma cell line | ATCC | HTB-36 |
| BeWo choriocarcinoma cell line | ATCC | CCL-98 |
| Primary Dermal Fibroblast; Normal, Human, Adult | ATCC | PCS-201-012 |

(*Continued on next page*)

*Continued*

| REAGENT or RESOURCE | SOURCE | IDENTIFIER |
|---|---|---|
| Software and Algorithms | | |
| Ensembl reference genome[53] | | |
| STAR 2.7.5a[54] | | |
| Subread v2.0.0[55] | | |
| R v4.0.3[56] | | |
| edgeR v3.34.0[57] | | |
| limma v3.48.1[58] | | |
| ComplexHeatmap v2.8.0[59] | | |
| ggplot2 v3.3.5[60] | | |
| enrichR v3.2[61–63] | | |
| SRA toolkit v2.11.0[64] | | |
| sva v3.50.0[65] | | |
| Cell Ranger v. 3.0.2 – Figure 2, v 5.0.1 – Figure 3 | 10x Genomics | |
| Seurat v4.0.3[66] | | |
| Clustree[67] | | |
| Slingshot (v2.10)[68] | | |
| miRDeep2 (v0.1.3)[69] | | |
| MACS2 v2.1.0[70] | | |
| SICER v1.1[71] | | |
| bcl2fastq2 v2.20 | Illumina | |
| bwa v0.7.12[72] | | |
| Samtools v0.1.19[73,74] | | |
| BEDtools v2.25.0[75] | | |
| wigToBigWig v4[76] | | |
| tidyverse v1.3.1[77] | | |
| DESeq-2 v1.42.0[78] | | |
| pheatmap v1.0.12[79] | | |
| Gviz v1.36.2[80] | | |
| biomaRt v2.48.2[81] | | |
| Other | | |
| Essential 8™ Medium | Thermo Fisher Scientific | A1517001 |
| StemPro™ Accutase™ Cell Dissociation Reagent | Thermo Fisher Scientific | A1110501 |
| CryoStor® CS10 | STEMCELL Technologies | 07930 |
| Essential 6 | Thermo Fisher Scientific | A1516401 |
| Eagle's Minimum Essential Medium (EMEM) (ATCC® 30-2003™) | ATCC | 30-2003 |
| Fetal Bovine Serum (FBS) | ATCC | 30-2020 |
| F-12K Medium (Kaighn's Modification of Ham's F-12 Medium) | ATCC | 30-2004 |
| DMEM/F-12, GlutaMAX™ supplement | Thermo Fisher Scientific | 10565018 |
| Dulbecco's Modified Eagle's Medium (DMEM) | ATCC | 30-2002 |
| Fetal Bovine Serum (FBS) | ATCC | 30-2020 |
| 24 Well Glass Bottom Plate with high performance #1.5 cover glass | Cellvis | P24-1.5H-N |
| pluriStrainer® 20 μm (Cell Strainer) | pluriSelect | 43-50020-03 |
| 96-well ImageLock plates | Sartorius | 4379 |

## EXPERIMENTAL MODEL AND STUDY PARTICIPANT DETAILS

### Cell lines and culture

All hESCs (WA07, WA09, WA14, and WA17; WiCell) and hiPSCs (JHU191i, JHU198i, and MCW032i; WiCell; WTC iPSC; Allen Institute for Cell Science) were maintained under feeder- and xeno-free conditions in Essential 8 (E8) medium (A1517001, Thermo Fisher Scientific) on microplates or T175 flasks coated with vitronectin (VTN; A14700, Thermo Fisher Scientific) at a concentration of 0.5 μg/cm$^2$. Cells were passaged every three days. The hPSC colonies were treated with 0.5 mM EDTA (15575020, Invitrogen) in phosphate buffered saline (PBS) without calcium or magnesium (14190144, Gibco) for 5-6 min to dissociate the hPSC colonies. The resulting cell clumps were counted using the Nexcelom Cellometer automated cell counter. The clumps were then plated at a density of 2-3 × 10$^5$ cells per cm$^2$ in E8 medium and maintained in a humidified atmosphere containing 5% $CO_2$ at 37°C. Where indicated, hPSC were cultured in presence of a cocktail of compounds 50 nM Chroman 1 (HY-15392, MedChemExpress), 5 μM Emricasan (S7775, Selleck Chemicals), 1× Polyamine Supplement (P8483-5ML, Millipore-Sigma), and 0.7 μM trans-ISRIB (5284, Tocris Biosciences) termed "CEPT", up to 24 h following passaging to enhance the viability of the cells. In the case of TSC culture, TE3 medium contains 25 nM Chroman 1 and this concentration is increased to 50 nM at each passage, with the remaining "EPT" components added for a full cocktail.

Human dermal fibroblasts (PCS-201-012, ATCC) were seeded on tissue culture-treated 6-well plates at a density of 5,000 cells/cm$^2$ in fibroblast basal medium (PCS-201-030, ATCC) supplemented with components of the Fibroblast Growth Kit, Low Serum (PCS-201-041, ATCC) and incubated in a humidified atmosphere at 37°C, 5% $CO_2$, and 21% $O_2$. Medium was changed daily, and the cells were passaged every three days by treatment with Accutase for 6 min, followed by dilution with culture medium, centrifugation at 200 g for 3 min, and replating onto 6-well plates.

Human CC cell lines JEG-3 (HTB-36, ATCC) and BeWo (CCL-98, ATCC) were seeded on tissue culture-treated 6-well plates at a density of 20,000 cells/cm$^2$ in Eagle's Minimum Essential Medium (30-2003, ATCC) and Kaighn's Modification of Ham's F-12 Medium (30-2004, ATCC), respectively. Both JEG-3 and BeWo cell lines were supplemented with 10% fetal bovine serum (FBS; 30-2020, ATCC). The cultures were incubated in a humidified atmosphere at 37°C, 5% $CO_2$, and 21% $O_2$. Medium was changed daily and the cells were passaged every three days by treatment with Accutase for 15 min, followed by dilution with culture medium, centrifugation at 200 g for 3 min, and replating onto 6-well plates.

## METHOD DETAILS

### Differentiation of hPSCs into TE and TSC

hPSC maintained in E8 medium on VTN-coated 6-well plates, as described above, were dissociated using 0.5 mM EDTA for 5-6 min. The resulting clumps were then counted using the Nexcelom Cellometer and seeded at a density of 4-5 × 10$^5$ per cm$^2$ in E8 medium on VTN-coated 6-well plates. 24 h later (day 0), the spent medium was replaced with TE1 medium and changed every day until day 3. On day 3, the medium was replaced with TE2 medium until day 7-10, with daily medium changes. Then the monolayers containing a mixture of mononucleated TE-like cells and multinucleated STB cells were partially dissociated using StemPro Accutase (A1110501, Gibco) for 8-12 minutes. The resulting clumps of cells were plated at a density of 2.5 × 10$^5$/cm$^2$ in TE3 medium supplemented with additional 25 nM of Chroman 1. 24 h later, the medium was changed with fresh TE3 medium with basal concentration of Chroman 1 (25 nM). The subsequent media changes were performed daily. The subsequent passaging steps were performed using Accutase treatment for 5-8 min. The seeding density remained at 2.5 × 10$^5$/cm$^2$ for an additional passage. Then the seeding density was increased to 3-4 × 10$^5$/cm$^2$ and remained the same for all passages on. The passaging interval was 3 days and the derived proliferative cell lines were passaged over 40 times. Cells were maintained in a humidified atmosphere containing 5% $CO_2$ at 37°C.

Where indicated, for the first 24 h of culture following passaging, the use of 50 nM of Chroman 1 was complemented with 5 μM Emricasan, polyamines, and 0.7 μM trans-ISRIB to make up the full CEPT cocktail for viability enhancement, as described above for the culture of hPSCs.

### Differentiation of TSCs into EVT and STB

For EVT differentiation, TSC were cultured in TE3 medium in hypoxia (2% $O_2$) for at least 1 passage (3 days). Then the cultures were dissociated with Accutase for 10-15 min and seeded at a density of 6 × 10$^5$/cm$^2$ in EVT medium on VTN-coated culture plates. After 2 days of culture, the cells were dissociated with Accutase, replated at a density of 2 × 10$^5$/cm$^2$ in EVT medium, and cultured for another 6 days. Some cell lines required additional passages with 6 days intervals. The EVT medium was changed every other day and the cells were incubated at 37°C, 5% $CO_2$, and 2% $O_2$.

For STB differentiation, TSC cultures were dissociated with Accutase for 5-8 min, seeded at a density of 4-5 × 10$^5$/cm$^2$ in STB medium, and cultured for 3-4 days at 37°C, 5% $CO_2$, and 21% $O_2$.

### Differentiation of hPSC into ectoderm, mesoderm, and endoderm

Differentiation of hPSC into endoderm was initiated using the STEMdiff™ Definitive Endoderm Kit, TeSR™-E8™ Optimized (05115, STEMCELL Technologies). Cells were plated at a density of 150,000 cells/cm$^2$ on 6-well plates in E8 media supplemented with 50 nM of the ROCK inhibitor Chroman 1. After reaching 50-60% confluency, cell culture media was switched to TeSR-E8 Pre-Differentiation media for 24 h at which the cells reached 70% confluency. After aspirating the culture medium, cells were dissociated into single cells by 10-15 min incubation with 0.5 mM EDTA (15575020, Thermo Fisher Scientific) in PBS without calcium or magnesium (14190144, Thermo Fisher Scientific) at 37°C and plated at a

density of 210,000 cells/cm$^2$ onto VTN-coated 6-well plates in TeSR-E8 Pre-Differentiation media supplemented with 50 nM Chroman 1. 24 h post plating, the cultures were rinsed with DMEM/F-12 (10565018, Gibco) and media was replaced with Medium 1 (STEMdiff Definitive Endoderm Basal Medium with STEMdiff Definitive Endoderm Supplement A and STEMdiff Definitive Endoderm Supplement B). The next day, cell culture media was exchanged with Medium 2 (STEMdiff Definitive Endoderm Basal Medium with STEMdiff Definitive Endoderm Supplement B). On days 3-5, cell culture media was changed daily with Medium 2 (STEMdiff Definitive Endoderm Basal Medium with STEMdiff Definitive Endoderm Supplement B). On day 5, cells were ready for end-point assay.

Mesoderm differentiation of hPSC was induced using the STEMdiff Mesoderm Induction Medium (05221, STEMCELL Technologies). Cells were plated at a density of 50,000 cells/cm$^2$ on VTN-coated 6-well plates in E8 media supplemented with 50 nM Chroman 1 and incubated for 24 h. On days 2-5, cell culture medium was replaced with STEMdiff Mesoderm Induction Medium. On day 5, cells were ready for end-point assay.

For ectoderm differentiation, hPSC were plated at a density of 50,000 cells/cm$^2$ on VTN-coated 6-well plates in E8 media supplemented with 50 nM Chroman 1. 24 h later, the cell culture media was switched to E6 (A1516401, Thermo Fisher Scientfic) supplemented with 100 nM LDN 193189 dihydrochloride (6053, Tocris) and 2 μM A83-01. Media was changed daily for 6 days. On day 7, cells were ready for end-point assay. For all differentiation protocols, cells were maintained at 37°C in a humidified atmosphere containing 5% $CO_2$ and 21% $O_2$.

### Cryopreservation

Both hPSC and TE cells were harvested using EDTA and Accutase, respectively, as described above. The cell suspensions were centrifuged at 200 g for 3 min and resuspended in CryoStor CS10 (210102, BioLife Solutions) and placed into -80°C freezer in CoolCell containers (432000, Corning) overnight, then placed into -150°C freezer for long-term storage.

### Immunocytochemistry

hPSC, hPSC-derived TE cells, and proliferative TSC lines were cultured as described above on glass-bottom multiwell plates (P24-1.5H-N, Cellvis). The cultures were fixed with 4% formaldehyde (28908, Thermo Fisher Scientific) in PBS for 20 min, followed by permeabilization with 0.2% Triton X-100 Surfact-Amps Detergent Solution (85111, Thermo Fisher Scientific) in PBS for 10 min. The only exception was sample preparation for HLA-G staining, which required fixation and permeabilization for 30 min with 100% methanol (322415, Millipore-Sigma) chilled to -20°C. Then the cultures were incubated with PBS supplemented with 0.2% bovine serum albumin (BSA; A9418, Millipore-Sigma) and 5% donkey serum (017-000-121, Jackson ImmunoResearch) for 1 h at RT, followed by incubation with primary antibodies overnight at 4°C. Secondary antibodies were incubated at 4°C for 2 h. Then the cultures were stained with 2 μM Hoechst 33342 (62249, Thermo Fisher Scientific) in PBS for 10 min before imaging on a Zeiss LSM 710 confocal microscope (most imaging experiments) or Leica DMi8 epifluorescent microscope (Figures 1B and 3). Primary and secondary antibodies used are summarized in the key resources table.

### Calcein AM and propidium iodide staining

TSCs were seeded onto VTN-coated tissue culture-treated 12-well plates at a density of 4 × 10$^5$/cm$^2$ and cultured in TE3 medium. 24 h following seeding, 2 μM Calcein AM, a component of the LIVE/DEAD™ Viability/Cytotoxicity Kit for mammalian cells (L3224, Thermo Fisher Scientific), and 1μg/ml propidium iodide (J66584-AB, Alfa Aesar) were added into each well without medium change to fluorescently mark viable and dead cells, respectively. Incucyte S3 was used for live-cell imaging of the cultures 30 min following staining and for image analysis. The percentage of dead cells out of all cells was then calculated.

### Periodic Acid-Schiff (PAS) staining

PAS staining was performed using the Periodic Acid-Schiff (PAS) Kit (395B, Millipore-Sigma). TE and TSC cultures were grown on VTN-coated 6-well plates in their respective media, with daily medium change, as described above. Then the cultures were fixed for 1 min with a solution of 28.8% formaldehyde and 10% ethanol (E7023, Millipore-Sigma) in water. The fixed cultures were washed with slowly running tap water for 1 min, treated with periodic acid for 5 min, and washed three times with distilled water. The cells were then treated with Schiff reagent for 15 min, washed with running tap water for 5 min, and then imaged using a Zeiss Axiovert microscope equipped with an Axiocam 506 color camera with no phase contrast applied.

### High-content imaging

High-content imaging followed the same sample preparation procedures as immunofluorescence, except the image acquisition was performed using the Opera Phenix Plus High-Content Screening System (PerkinElmer) and confocal image analysis was performed using the Columbus Image Analysis System (PerkinElmer).

To measure the fusion index of TSCs differentiated into STB, fluorescent images were taken on the high-content imaging platform Opera Phenix (PerkinElmer). Image analysis was performed using the online interface of the Columbus software (PerkinElmer). ZO-1 (TJP1) expression was used to guide the categorization of cells into mononucleated and multinucleated. CGA expression was used to guide the identification of multinucleated cells. A total of 225 fields across two wells were analyzed. Fusion index was calculated as the percentage of nuclei found in multinucleated cells out of all nuclei.

### Time-lapse video microscopy

hPSC were differentiated into TE on VTN-coated Incucyte ImageLock 96-well plates (4379, Sartorius) according to the TE differentiation protocol described above. On day 5, plates were transferred into the IncuCyte S3 (Sartorius) and images were taken every 4 h over the course of 9-14 days.

### Transmission electron microscopy

hPSCs differentiating into TE/TB at different time points were fixed with glutaraldehyde in cacodylate buffer prepared by the Electron Microscopy Core at the Center for Cancer Research (National Cancer Institute at Frederick) for 24 h and further processed and imaged at the same facility.

### Flow cytometry

Cultures of hESC, TE (D10) and TSC were dissociated into single cell using Accutase (ThermoFisher Scientific) at 37°C for 5-10 min. The cells were subsequently washed with Cell Staining Buffer (420201, Biolegend) and incubated either in Cell Staining Buffer (unstained), fluorophore-conjugated isotype controls ( 5 μL/1x$10^6$ cells in 100 μL buffer) or fluorophore-conjugated antibodies (same concentration) at 4°C for 30 min. The cells were then washed twice with staining buffer and fixed with Cyto-Fast Fix Perm Solution from the Cyto-Fast Fix/Perm Buffer Set (426803, Biolegend) at room temperature for 20 min. After fixing, the cells were washed with Cyto-Fast Perm Wash Solution twice and resuspended in 500 μL Cell Staining Buffer. The fluorescence data were collected using the SH800S Cell Analyzer (Sony Corp.). The isotype controls and antibodies used are summarized in key resources table.

### Western blot

The automated, capillary-based Western blotting system Wes (ProteinSimple) was used according to the manufacturer's instructions. Briefly, cells were lysed in RIPA Lysis and Extraction Buffer (89901, Thermo Fisher Scientific) supplemented with cOmplete™, Mini Protease Inhibitor Cocktail (04-693-124-001, Roche), assisted by sonication. Lysates were cleared of debris by centrifugation at 14,000 g for 15 min. The protein content in lysates was determined using Pierce™ BCA Protein Assay Kit (23225, Thermo Fisher Scientific) according to the manufacturer's instructions. Lysates were diluted 1:4 with 1× sample buffer (ProteinSimple). The capillary cartridges of the 12-230 kDa Separation Module (SM-W003, ProteinSimple) were used, along with Anti-Rabbit (DM-001, ProteinSimple) and Anti-Mouse (DM-002, ProteinSimple) Detection Modules containing reagents and HRP-conjugated secondary antibodies. The detected chemiluminescent signal data were analyzed using the ProteinSimple Compass software. All western blot data were displayed by lanes in virtual blot-like images. Primary antibodies used are listed in key resources table.

### qRT-PCR

Cultures of human dermal fibroblasts, JEG-3 CC cells, and hPSC-derived TSCs were grown in 6-well plates. Cell culture medium was aspirated from the wells, the cells were washed twice with PBS, and the cell monolayers were lysed with Buffer RLT Plus supplemented with BME. RNA was extracted and purified using an RNeasy Plus Mini Kit (74136, Qiagen) according to the manufacturer's instructions. cDNA was synthesized from 500 ng of total RNA using a High-Capacity RNA-to-cDNA™ Kit (4388950, Thermo Fisher Scientific). PrimeTime Std® qPCR Assays (Integrated DNA Technologies) were used, according to manufacturer's instructions, as sets of primers and probes against gene targets. The instrument used was QuantStudio 12K Flex Real-Time PCR System (Thermo Fisher Scientific). Each reaction was performed in a final volume of 10 μl, consisting of 5 μl of 2× PrimeTime® Gene Expression Master Mix (1055771, Integrated DNA Technologies), 0.5 μl of 20× primer/probe suspension and 4.5 μl of cDNA diluted in DNase/RNase-free water (10977015, Thermo Fisher Scientific). The thermocycler program consisted of an initial UDG incubation at 50°C for 2 min, enzyme activation at 95°C for 10min, followed by 40 cycles at 95°C for 15 s and 60°C for 30 s. To confirm product specificity, melting curve analysis was performed after each amplification. GAPDH was used as a housekeeping gene. List of all primer probes is provided the key resources table.

### Bulk RNA-seq

Pluripotent cells, hPSC-derived TE cells, and proliferative TSC cultures were lysed using Buffer RLT Plus (1053393, Qiagen) supplemented with 2-mercaptoethanol (BME; 63689, Millipore-Sigma) directly in wells and RNA was extracted and purified using RNeasy Plus Mini Kit (74136, Qiagen) according to the manufacturer's instruction. QIAcube Connect automated workstation was used for the extraction (Qiagen). Genomic DNA was eliminated by both the gDNA eliminator column and on-column incubation with DNase I (79256, Qiagen). RNA concentration and integrity was determined using RNA ScreenTape (5067-5576, Agilent Technologies) on the instrument 4200 TapeStation System (Agilent Technologies). All samples had the RNA Integrity Number (RIN) greater than 9.5. Figure 1 sequencing libraries were constructed using TruSeq® Stranded mRNA Library Prep (20020595, Illumina) kit. Figure 2 sequencing libraries were constructed using TruSeq® Stranded Total RNA Library Prep (20020597, Illumina) kit at the National Cancer Institute's Center for Cancer Research sequencing core facility. The libraries were then sequenced at the same facility using the Illumina HiSeq system (Figure 1) and the NovaSeq 6000 system (Figure 2).

Bulk RNA-seq libraries for Figure 3 were constructed and sequenced in-house. In brief, 1 μg of purified RNA per sample was used to generate sequencing libraries following the manufacturer's protocols of KAPA mRNA HyperPrep Kit (KK8581, Roche Life Science). The libraries were indexed using KAPA Unique Dual-Indexed Adapter Kit at 7 μM (KK8727, Roche Life Science) and 7 cycles of PCR library

amplification were used. The sample preparation procedure was carried out using Biomek i7 Automated Workstation (Beckman Coulter) and the automation protocol was validated by Roche Life Science. Libraries were then quantified on a QuantStudio Real-Time PCR System (A34322, Applied Biosystems) using the KAPA Library Quantification Kit for Illumina Platforms (KK4824, Roche Life Science). The libraries were individually normalized to 4 nM by diluting each library with 10 mM Tris-HCl (pH 8.5; T1062, Teknova) prior to pooling. The pooled libraries were then quantified according to the manufacturer's instruction and diluted to 1.5 nM for sequencing. Sequencing was performed on Illumina NovaSeq 6000 system using NovaSeq 6000 S4 Reagent Kit v1, 300 cycle (20012866, Illumina), with 300 pM as the final loading concentration.

Raw FASTQ files were aligned to the human reference genome[1] (CRCh38 primary assembly, Ensembl annotation version 100) using STAR[2] (version 2.7.5a). Counts were derived from the aligned reads using featureCounts from the Subread suite[3] (v 2.0.0). The counts were processed in R[4] (version 4.0.3) using package edgeR (version 3.34.0).[5] Filtering of genes with low counts, normalization, multidimensional scaling (MDS) plot construction and Differential expression analysis were performed using limma (version 3.48.1).[6] Heatmaps were constructed using ComplexHeatmap (version 2.8.0).[7] Expression plots were constructed using ggplot2 (v3.3.5).[8] Gene set enrichment analysis was performed in R using Enrichr (package "enrichR").[9–11] The analysis scripts are available at https://github.com/cemalley/Slamecka_methods.

For the purpose of comparison of RNA-seq transcriptional profiles obtained as part of this study and external laboratories, raw data in form of FASTQ files was downloaded from the Sequence Read Archive (SRA)[12] using the command fasterq-dump from the SRA toolkit (v2.11.0). The mapping/alignment and feature counting were performed using the same workflow, the same versions of reference genome and software versions, as were used for the datasets presented in this study. Then the counts were collectively loaded into R using edgeR and the batch effect was removed using ComBat-seq from package sva (v3.50.0)[65], applying it to the raw, unfiltered counts by supplying the batch variable. No group variable was specified. Then the counts were filtered, normalized, and MDS plots were constructed using limma. All computationally intensive operations for all analyses presented in this manuscript were performed on the NIH's Linux-based high-performance computing platform Biowulf.

### PluriTest

FASTQ files corresponding to RNA-seq samples were first downsampled so that the file sizes did not exceed 1.5 GB, a prerequisite for the web-based analysis. The FASTQ files were then uploaded to https://www.pluritest.org for analysis in pair-end mode.

### scRNA-seq

Single-cell suspensions from hPSC, D3, D6 TE cells, and TSC were obtained after a 15 min Accutase treatment; and from D9 TE cells after 20-25 min. Cells were suspended in PBS+0.04% BSA and cell clumps were mitigated by passing the suspension through the cell strainer pluriStrainer® with pore size of 20 μm (43-50020-03, pluriSelect). Gel Bead-In Emulsion (GEM) generation, cDNA synthesis, and sequencing library preparation was performed in-house using Chromium Single Cell 3' Library & Gel Bead Kit version 2 (120237, 10X Genomics) and Chromium Single Cell A Chip Kit (120236, 10X Genomics). Figure 3 single-cell sequencing libraries were prepared using Chromium Single Cell 3' GEM, Library & Gel Bead Kit version 3 (1000075, 10X Genomics) and Chromium Single Cell B Chip Kit (1000073, 10X Genomics). Sample indexing for both scRNA-seq experiments was performed using Chromium i7 Multiplex Kit (120262, 10X Genomics). To determine the concentration, integrity, and size distribution of fragments during the procedure, cDNA trace analysis was performed using High-Sensitivity D5000 ScreenTape (5067-5588, Agilent Technologies) and library trace analysis was performed using High-Sensitivity D100 ScreenTape (5067-5582, Agilent Technologies) on the 4200 TapeStation System (Agilent Technologies). The prepared libraries for the Figure 2 dataset were sequenced using the NovaSeq 6000 at the National Cancer Institute's Center for Cancer Research sequencing core facility. The Figure 3 dataset single-cell sequencing libraries were sequenced in-house using the NovaSeq 6000. scRNA-seq parameters are summarized in Table S8 (supplemental information) and include sample indices, numbers of cDNA reverse transcription (RT) cycles, and numbers of targeted and recovered cells.

BCL files produced by the Illumina sequencer were converted to FASTQ files using command mkfastq from the Cell Ranger analysis toolkit (v. 3.0.2 – Figure 2, v 5.0.1 – Figure 3 and 10X Genomics). The FASTQ files were processed with Cell Ranger count to produce count matrices suitable for analysis in R using package Seurat[13] (v. 4.0.3). Clustree[14] was used to guide the selection of cluster resolution. Seurat was also used for integration with previously published datasets. For trajectory analysis, the R package Slingshot[15] was used. The analysis scripts are available at https://github.com/cemalley/Slamecka_methods.

### miRNA-seq

Total RNA of each sample was extracted from cell pellets using QIAzol Lysis Reagent (79306, Qiagen) and used to prepare the miRNA sequencing library. The assay and a part of the data analysis was performed by Arraystar Inc. After the completed libraries were quantified with the Agilent 2100 Bioanalyzer, the DNA fragments in the libraries were denatured with 0.1M NaOH (72068, Millipore-Sigma) to generate single-stranded DNA molecules.

For RNA quality control, agarose gel electrophoresis was used to check the integrality of total RNA samples. NanoDrop ND-1000 instrument was used for the measurement of concentration (abs 260) and protein contamination (ratio abs260/abs230) of total RNA samples.

### *Library preparation*

Reagents: NEBNext Poly(A) mRNA Magnetic Isolation Module (New England Biolabs); RiboZero Magnetic Gold Kit (Human/Mouse/Rat) (Epicentre, an Illumina Company); NEBNext Small RNA Library Prep Set for Illumina (E7330L, New England Biolabs).

Total RNA of each sample was used to prepare the miRNA sequencing library, which included the following steps.

(1) 3′-adaptor ligation
(2) 5′-adaptor ligation
(3) cDNA synthesis
(4) PCR amplification
(5) size selection of 135– - 155 bp PCR amplified fragments (corresponding to 15 – 35 nt small RNAs). The libraries were denatured as single-stranded DNA molecules, captured on Illumina flow cells, amplified *in situ* as clusters, and finally sequenced for 51 cycles on Illumina NextSeq per the manufacturer's instructions.

### *Sequencing*

The DNA fragments in well mixed libraries were denatured to generate single-stranded DNA molecules, loaded onto channels of the flow cell at a concentration of 8 pM, and amplified *in situ* using TruSeq Rapid SR Cluster Kit (#GD-402-4001, Illumina). Sequencing was carried out using the Illumina NextSeq 500 according to the manufacturer's instructions. Sequencing was carried out by running 51 cycles.

### *Sequencing quality control*

Raw data files in FASTQ format were generated from the Illumina sequencer. To examine the sequencing quality, the quality score plot of each sample was plotted. Quality score Q is logarithmically related to the base calling error probability (P):

$$Q = -10\log_{10} P$$

### *miRNA-seq data analysis workflow*

Raw sequencing data generated from Illumina NextSeq 500 that pass the Illumina chastity filter are used for following analysis. Trimmed reads (trimmed 3′-adaptor bases) were aligned to reference genome.

### *Quality assessment of sequencing library*

Agilent 2100 Bioanalyzer was used for assessment of the quality of sequencing library. Library concentration was determined by qPCR method.

### *Mapping summary*

After quality control, the reads were 3′-adaptor trimmed and filtered $\leq$15 bp reads with cutadapt software. The trimmed reads were aligned to reference genome with bowtie software. The reads statistical information is listed in the table below. In a typical experiment, it is possible to align 40–90% of the reads to the reference genome. However, this percentage depends on multiple factors, including sample quality, library quality, and sequencing quality.

### *miRNA expression results*

The expression level (Reads count) of miRNA were calculated using miRDeep2.[16] The number of identified miRNA per group was calculated based on the mean of CPM in group $\geq$1. Counts per million reads (CPM) is calculated with the formula:

$$CPM = \frac{C \times 10^6}{N}$$

C: The count of reads that map to a certain gene/transcript.
N: The total reads count that map to all genes/transcript.

### *Additional miRNA-seq analysis steps performed internally*

The counts were processed in R (version 4.0.3) using package edgeR (version 3.34.0). Normalization, MDS plot construction, and differential expression analysis were performed using limma (version 3.48.1). Heatmaps were constructed using ComplexHeatmap (version 2.8.0).

## MeDIP-seq

The assay and a part of the data analysis was performed by Active Motif. The samples were delivered to Active Motif as flash-frozen cell pellets on dry ice. DNA was extracted, then sonicated to ~150–300 bp, and Illumina adapters were ligated to the DNA ends. This DNA was then used in immunoprecipitation (IP) reactions using 5-Methylcytosine (5-mC) mouse monoclonal antibody (39649, Active Motif). Immunoprecipitated

DNA and input control (pooled DNA that did not go through the IP step) were finally processed into sequencing libraries using PrepX DNA Library Kit (400075, Takara) and sequenced using the Illumina platform (NextSeq 500, 75-nt single-end).

### *Description of analysis steps performed by Active Motif*

(1) Sequence Analysis: The 75-nt single-end (SE75) sequence reads generated by Illumina sequencing (using NextSeq 500) were mapped to the genome using the BWA algorithm ("bwa aln/samse" with default settings). Alignment information for each read was stored in the BAM format. Only reads that passed Illumina's purity filter, aligned with no more than 2 mismatches, and mapped uniquely to the genome were used in the subsequent analysis. In addition, duplicate reads were removed.

(2) Determination of Fragment Density: Since the 5′-ends of the aligned reads ("tags") represent the end of ChIP/IP-fragments, the tags were extended in silico (using Active Motif software) at their 3′-ends to a length of 200 bp, which corresponded to the average fragment length in the size-selected library. To identify the density of fragments (extended tags) along the genome, the genome was divided into 32-nt bins and the number of fragments in each bin was determined. This information ("signal map"; histogram of fragment densities) was stored in a bigWig file, which could be visualized in genome browsers. bigWig files also provided the peak metrics in the Active Motif analysis program described below.

(3) Peak Finding: The generic term "Interval" is used to describe genomic regions with local enrichments in tag numbers. Intervals were defined by the chromosome number and a start and end coordinate. The two main peak callers used were MACS/MACS2[17] and SICER.[18] MACS is suitable to identify the binding sites of transcription factors that bind to discrete sites (often containing a consensus DNA sequence) as well as many active histone marks and methyl-C enriched regions, while SICER is used to study proteins that bind to extended regions in the genome (such as repressive histone marks or RNA polymerase II). Both methods look for significant enrichments in the ChIP/IP data file when compared to the Input data file or relative to neighboring background regions.

(4) Additional Analysis Steps - Normalization: The tag number of all samples (within a comparison group) was reduced by random sampling to the number of tags present in the smallest sample. This normalization method works well for most assays where the majority of tags map to background (i.e., non-peak) regions, and it can detect site-specific as well as global differences in target enrichments between samples.

(5) Merged Region Analysis: To compare peak metrics between 2 or more samples, overlapping Intervals were grouped into "Merged Regions", which are defined by the start coordinate of the most upstream Interval and the end coordinate of the most downstream Interval (union of overlapping Intervals; "merged peaks"). In locations where only one sample has an Interval, this Interval defines the Merged Region. The use of Merged Regions is necessary because the locations and lengths of Intervals are rarely the same when comparing different samples. Furthermore, with this approach fragment density values can be obtained even for samples for which no peak was called.

(6) Annotations: After defining the Intervals and Merged Regions, their genomic locations along with their proximities to gene annotations and other genomic features were determined. In addition, average and peak (i.e., at "summit") fragment densities within Intervals and Merged Regions were compiled.

### *MeDIP-seq analysis software versions used at Active Motif*

bcl2fastq2 (v2.20): processing of Illumina base-call data and demultiplexing.
bwa[19] (v0.7.12): alignment of reads to reference genome.
Samtools[20,21] (v0.1.19): processing of BAM files.
BEDtools[22] (v2.25.0): processing of BED files.
MACS2 (v2.1.0): peak calling; narrow peaks.
SICER (v1.1): peak calling: broad peaks.
wigToBigWig[23] (v4): generation of bigWIG files.

### *Additional MeDIP-seq analysis steps performed internally*

To conservatively assess differential methylation, only those peaks supported by at least two biological replicates were retained for downstream analysis using basic filtering and chaining with dplyr (tidyverse[24] v1.3.1) in R. DESeq-2[25] (v1.42.0) with default parameters was then used to perform differential methylation analysis to which the filtered MeDIP-Seq normalized peak counts were supplied. Manhattan plots were generated in ggplot2[8] (v3.3.5). Top 20 significantly differentially methylated peaks were highlighted. Heatmaps were created using pheatmap[26] (v1.0.12) by plotting the unscaled $\log_2$(count +1) for the top 50 peaks sorted by the absolute value of the $\log_2$(fold-change). We annotated the sample type using the options for annotation_col and annotation_colors in pheatmap. Locus zoom plots were built using Gviz (v 1.36.2)[80] by creating and combing ideogram tracks, biomaRt (v2.48.2)[81] generated annotation tracks, custom annotation tracks for identified MeDIP-Seq peaks, gene axis tracks and count data tracks highlighting approximate promoter regions (1000 bp upstream of the transcriptional start site), and significant differentially methylated peaks within the specified locus. Count data for long arm of chromosome 21 was extracted from BAM files for each sample and replicate. Then the data was split into 40 numbered bins and a histogram was generated in ggplot2 (v3.3.5).

### Pregnancy test

The spent medium of TE cells differentiated from hPSC at D10 (cultured in TE2 medium) was loaded into the cassette of a commercially available over-the-counter Alere hCG Urine II Test Kit for detection of hCG. The hCG detection threshold is 20 mIU/mL according to the manufacturer (Abbott).

### Secretome analysis

WA09 ESCs (D4) and WA09-derived TE cells (D10) were grown in VTN-coated 6-well plates at 37°C in a humidified atmosphere containing 5% $CO_2$ and 21% $O_2$. A total of 8 mL of spent medium was collected from 4 wells of a 6-well plate after 24 h. The medium was then frozen at −80°C and shipped to Applied Biomics for analysis using the nanoscale liquid chromatography coupled to tandem mass spectrometry (Nano LC-MS/MS) method. The main steps performed were protein fractionation, reduction, alkylation, trypsin digestion, and Nano HPLC. Ion composition was then detected by MS/MS and a database search was then performed to identify the proteins.

## QUANTIFICATION AND STATISTICAL ANALYSIS

Data are presented as the mean ± SD. Statistical analyses (R ggplot2) were performed using different tests as appropriate and as described in figure legends.